

## Water Resources Research

### RESEARCH ARTICLE

10.1029/2018WR022842

#### Key Points:

- A distributed hydrologic model is tested with long-term measurements of water and energy states and fluxes in a piedmont slope watershed
- When modified to account for transient channel losses, the model reproduces well the percolation estimates and observed streamflow response
- Modeling scenarios reveal the relative importance of hillslope and channel properties on runoff generation and percolation losses

#### Correspondence to:

E. R. Vivoni,  
vivoni@asu.edu

#### Citation:

Schreiner-McGraw, A. P., & Vivoni, E. R. (2018). On the sensitivity of hillslope runoff and channel transmission losses in arid piedmont slopes. *Water Resources Research*, 54, 4498–4518. <https://doi.org/10.1029/2018WR022842>


Received 27 FEB 2018

Accepted 12 JUN 2018

Accepted article online 20 JUN 2018

Published online 4 JUL 2018

## On the Sensitivity of Hillslope Runoff and Channel Transmission Losses in Arid Piedmont Slopes

Adam P. Schreiner-McGraw<sup>1</sup> and Enrique R. Vivoni<sup>1,2</sup> 

<sup>1</sup>School of Earth and Space Exploration, Arizona State University, Tempe, AZ, USA, <sup>2</sup>School of Sustainable Engineering and the Built Environment, Arizona State University, Tempe, AZ, USA

**Abstract** Channel transmission losses alter the streamflow response of arid and semiarid watersheds and promote focused groundwater recharge. This process has been primarily studied in dryland channels draining large areas that are displaced away from hillslope runoff generation. In contrast, small watersheds on arid piedmont slopes allow the investigation of interactive hillslope and channel processes that control the partitioning between surface and subsurface flows. In this study, we utilize high-resolution, long-term measurements of water balance components in an instrumented watershed of the Chihuahuan Desert to set up, parameterize, and test a process-based, distributed hydrologic model modified to account for channel losses. A transient method for capturing capillary effects in channels results in simulations with a reliable representation of the watershed energy balance, soil moisture dynamics, hillslope infiltration, channel transmission (or percolation) losses, and streamflow yield over the study period. The simulation also reproduces a conceptual model of hillslope infiltration-excess runoff generation linked to downstream channel percolation losses that depend on the rainfall event size. Model-derived thresholds were obtained for the amount of hillslope runoff (6 mm) and rainfall (12.5 mm) necessary for streamflow yield, such that 40% of percolation occurs for small events that do not reach the outlet. Using a set of scenarios, we identify that hillslope infiltration controls the rainfall threshold necessary to initiate percolation, while channel infiltration affects the partitioning into percolation and streamflow yield. Thus, the connectivity along hillslope-channel pathways is deemed an essential control on the streamflow generation and groundwater recharge in arid regions with complex terrain.

### 1. Introduction

A large component of groundwater recharge in arid and semiarid regions originates as transmission losses in ephemeral rills and channels (e.g., Abdulrazzak, 1995; Goodrich et al., 2004; McCallum et al., 2014; Shanafield & Cook, 2014; Wainwright et al., 2002). Infiltration of streamflow occurring through fluvial features depends on the hydraulic conductivity of the variably saturated sediments and the local hydraulic head (Niswonger et al., 2005; Parsons et al., 1999; Shentsis & Rosenthal, 2003; Sorman & Abdulrazzak, 1993; Villeneuve et al., 2015). Transmission losses have generally been studied by monitoring natural flow events in large dryland channels (Pool, 2005; Walters, 1990) or through field experiments performed on small plots or rills (Parsons et al., 1999; Wainwright et al., 2000). Detailed comparisons of event-based infiltration losses across different landform units (e.g., mountain block, alluvial surfaces, fluvial channels, and playas) have not received much attention, though prior efforts suggest that higher losses in channel features are typical as compared to hillslope surfaces (Abrahams et al., 2006). Furthermore, understanding the hydrologic connectivity between hillslopes and channels is important for determining infiltration losses, which are commonly used as proxies for groundwater recharge due to the occurrence of deep vadose zones (Wilson & Guan, 2004).

The hydrologic connectivity between upland hillslopes and downstream channels has been the subject of broad interest in many climatic settings (e.g., Frisbee et al., 2007; Gutiérrez-Jurado et al., 2007; Jencso et al., 2009; Lin et al., 2006; Puigdefabregas et al., 1998; Sidle et al., 2000). In comparison to more humid areas, the interaction between hillslopes and channels is more limited in arid and semiarid climates (Osborn & Renard, 1970; Yair & Lavee, 1985). This is because overall dry antecedent conditions promote high infiltration losses along surface and subsurface pathways when sufficiently large storm events lead to their connectivity (cf. Tooth, 2000). Few studies have been aimed at understanding the relative roles of hillslope and channel processes on watershed-scale runoff generation and their implication on transmission losses (or percolation, Schreiner-McGraw & Vivoni, 2017) in dryland systems. For instance, Puigdefabregas et al. (1998) found that

semiarid hillslopes in Spain mainly contributed to runoff through the infiltration-excess mechanism occurring during intense but short storms and had a limited role in the recharge generated during longer-lasting storms in downstream channel areas. Through a conceptual modeling approach, Kirkby et al. (2002) explored the varying roles of semiarid hillslope properties on downstream runoff, indicating the importance of hillslope-channel connectivity and the losses within these features in understanding the small catchment response to storm events. Similarly, Goodrich et al. (1997) found a threshold in area (37–60 ha at the semiarid Walnut Gulch, Arizona) at which a transition occurred in the dominant mechanism impacting the watershed response from hillslope infiltration to channel transmission losses.

While channel transmission losses have long been recognized as an important process in arid and semiarid watersheds, the primary focus has generally been on large alluvial channels transporting runoff from mountain areas, often termed as mountain front recharge (Manning & Solomon, 2003; Wilson & Guan, 2004). Piedmont slopes associated with mountain fronts have traditionally been considered primarily as transport surfaces for episodic streamflow generated on mountain blocks (e.g., Mukhopadhyay et al., 2003; Pelletier et al., 2005; Robins et al., 2009). As a result, there has been little attention paid to the role of piedmont slopes and their associated watersheds with interconnected systems of channels and hillslopes as potential recharge sources. For instance, the water budget of the Walnut Gulch, Arizona (Renard et al., 2008, their Figure 5), does not recognize piedmont slope recharge (other than in large channels) and instead indicates that infiltration into hillslope surfaces and small channels is consumed by evapotranspiration (ET). However, observations of Scott et al. (2000) and Coes and Pool (2005) in the Walnut Gulch lend support to the occurrence of recharge down to about 2-m depths on hillslope soils. As a result, the conceptual model elaborated by Renard et al. (2008) suggests that small watersheds on piedmont slopes do not support transmission losses despite evidence of its occurrence on hillslope soils. This might be due to other findings indicating that recharge on flat surfaces of arid and semiarid regions is negligible due to the efficient consumption of infiltration by vegetation (e.g., Gee et al., 1994; Scanlon et al., 1999; Seyfried et al., 2005; S. D. Smith, Herr, et al., 1995).

Nevertheless, recent observations in an arid piedmont watershed indicate that infiltration losses from hillslope surfaces and transmission losses in first-order channels account for a large fraction of the water balance (Schreiner-McGraw & Vivoni, 2017). Monthly losses from the small watershed (4.7 ha) were estimated using coordinated measurements of precipitation, streamflow, ET, and changes in soil water storage over a 6-year period (2010–2016). A water balance residual of 26% of the total precipitation was found and attributed to subsurface losses, with wetter-than-average summer seasons playing an important role. The observations were then utilized to generate a conceptual model of hydrologic connectivity accounting for infiltration-excess runoff from hillslope surfaces and channel transmission losses. Central to the conceptual model is that a threshold in channel storage capacity needs to be exceeded such that hillslope runoff generation leads to streamflow yield from the watershed. These findings are consistent with prior work hypothesizing that piedmont slope watersheds with coarse or gravelly soil textures are disconnected to downstream areas due to their subsurface losses (Bestelmeyer et al., 2011; Snyder et al., 2006). Due to current limits in the observational network, however, uncertainty remains with respect to the relative roles played by hillslope surfaces and channel reaches on runoff generation and subsurface losses in the watershed.

A useful approach to quantify the effects of hillslope and channel properties on the watershed response is through the use of numerical models incorporating the relevant hydrologic processes (e.g., Goodrich et al., 1997; Howes & Abrahams, 2003; Kirkby et al., 2002). Process-based, distributed hydrologic models are particularly useful for this endeavor since this approach aims to (1) resolve hillslope and channel features at high resolution, (2) capture the hydrologic connectivity and dynamic interaction of hillslopes and channels, and (3) account for the spatial distribution of soil and vegetation properties and antecedent wetness conditions (cf. Mahmood & Vivoni, 2011; Méndez-Barroso et al., 2016). For arid and semiarid regions, an essential model component is to account for transmission losses in the channel network using one of a number of possible numerical methods (e.g., Abdulrazzak & Morel-Seytoux, 1983; Lane, 1982; Rew & McCuen, 2010; Schoener, 2017; R. E. Smith, Goodrich, et al., 1995). Costa et al. (2012) provide an excellent review of the modeling approaches available for channel transmission losses in disconnected losing streams that are typical of small dryland watersheds. Furthermore, Costa et al. (2012) point to the need for integrating transmission loss modules as a component of catchment-scale hydrologic models that represent multiple processes within arid and semiarid regions and can be tested against spatially intensive hydrologic observations.

In this study, we utilize a process-based hydrologic model in a first-order piedmont slope watershed at the Jornada Experimental Range (JER) to explore the sensitivity of hillslope runoff and channel transmission losses to variations in watershed properties. Our approach is based on modifications to the Triangulated Irregular Network (TIN)-based Real-time Integrated Basin Simulator (tRIBS, Ivanov et al., 2004; Vivoni et al., 2007, 2011) to account for transmission (percolation) losses in dry, ephemeral channels. The model application and performance evaluation is based on using extensive field sampling and an environmental sensor network over a 6-year period (1 July 2010 to 30 September 2016), supplemented with remote sensing data from a ground-based camera, unmanned aerial vehicle (UAV), and satellite platforms (Schreiner-McGraw et al., 2016; Templeton et al., 2014). A particular focus is placed on representing the spatial distribution of vegetation species and bare soil areas, as well as the temporal variation of vegetation properties, occurring upon the terrain that describes the interconnected hillslope-channel system. Model performance is evaluated against continuous, high temporal resolution data from the environmental sensor network, including an eddy covariance (EC) tower, a set of soil moisture sensor profiles located in different hillslope and channel locations, and an outlet runoff flume. The split-sample calibration and validation includes evaluations of monthly percolation losses occurring in the main channel for a set of different loss algorithms implemented in the model (Blasch et al., 2006; Schoener, 2017). Furthermore, the simulation outcomes are evaluated with streamflow metrics from the outlet flume that were not used directly in the model calibration. Finally, we investigate the relative effects that hillslope and channel properties have on channel percolation through a series of scenarios that independently and jointly vary parameter values around their calibrated or observed amounts.

## 2. Methods

### 2.1. Study Site Characteristics and Field Sampling

The study site is located in south central New Mexico, United States, at the JER, which has been an active experimental rangeland since 1912 and part of the Long Term Ecological Research network since 1982 (see Havstad et al., 2006). The regional topography is composed of north-south trending mountain ranges with broad intervening valleys produced by the Rio Grande rift tectonic system (Monger et al., 2006; Peterson, 1981). Major physiographic features in the JER consist of the San Andrés Mountains to the east and its piedmont slope (or bajada) draining westward toward the endorheic basin floor (Figure 1). The focus of this work is on the piedmont slope that consists of a complex assemblage of landforms (e.g., alluvial fan collars, ballenas, interfan valleys, and fan piedmonts) with coarse alluvial deposits (see Rachal et al., 2012; Wondzell et al., 1996) where the depth to the regional groundwater table ranges from 90 to 105 m (King & Hawley, 1975). We focus on this physiographic division due to the long-term observational studies performed by the Jornada Long Term Ecological Research in a small watershed (4.7 ha or 0.047 km<sup>2</sup>) on an alluvial fan remnant (Monger et al., 2006) since 1977 (Tromble, 1988; Turnbull et al., 2013) and more intensively since 2010 (e.g., Vivoni, 2012; Vivoni et al., 2014).

High-resolution imagery from a set of UAV flights was used by Templeton et al. (2014) along with field sampling to characterize the bare earth terrain and hydrographic properties of the watershed at 1-m resolution (see Table 1). Figure 1 depicts the digital elevation model (DEM) of the watershed and its hydrographic characteristics derived from terrain analyses and aided by a field survey using a differential Global Positioning System. A channel consisting of a mixture of sands and gravel (>1.5 m in depth) drains westward in accordance with the piedmont slope, dividing the watershed into three principal units (north facing, south facing, and west facing slopes). Hillslope soils are classified as Middle Tank Gravelly Soil (Monger, 2006) and are sandy loam in texture with high gravel contents and a calcium carbonate layer located at depths ranging from 30 to 50 cm throughout the sampling sites on the hillslope surfaces (see Anderson & Vivoni, 2016). In contrast, channel sediments are sandy in texture with the presence of large cobbles at depth. The main channel is about 400 m in length, ranges from 0.5 to 1 m in width and has several small tributaries (see Schreiner-McGraw & Vivoni, 2017, for subwatershed properties). Channel width ( $W_c$  in meter) estimates at varying drainage areas ( $A_d$  in square kilometer) were used to obtain a relation  $W_c = 3.59A_d^{0.35}$  applicable to the channel network. A double ring infiltrometer was used to measure the saturated hydraulic conductivity at seven locations along the main channel length.

Climate at the study site is classified as desert (Köppen zone BWk, Wainwright, 2006), with a mean annual rainfall of 257 mm/year and mean annual temperature of 15.3 °C (2010–2016). As a result of woody plant encroachment in various phases (Gibbens et al., 2005), a mixed shrubland characterizes the watershed,

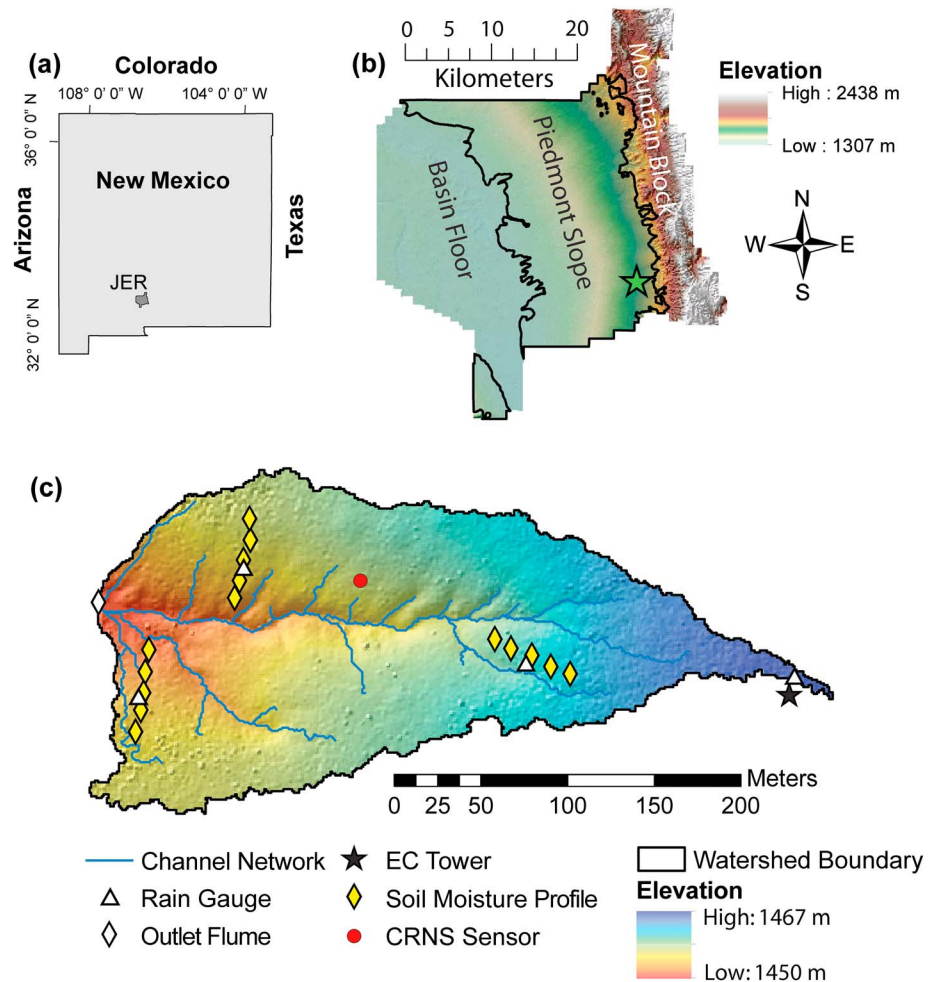


**Figure 1.** (a) Study site location. (b) The 10-m digital elevation model of the Jornada Experimental Range with three landform units and watershed (star). (c) The 1-m bare earth digital elevation model of the watershed, its boundary, and channel network derived from a differential Global Positioning System survey. Instrument locations are also shown in (c). JER = Jornada Experimental Range; EC = eddy covariance; CRNS = cosmic ray neutron sensor.

**Table 1**  
Watershed and Channel Properties

Property (unit)	Descriptor	Value
Watershed Area (m <sup>2</sup> )		46,734
Elevation (m)	Mean	1,458
	Max.	1,467
	Min.	1,450
Slope (degree)	Mean	3.9
	Max.	45
	Min.	0
Drainage density (m <sup>-1</sup> )		0.03
Channel surface area (m <sup>2</sup> )		675
Channel initiation threshold (m <sup>2</sup> )		721
Channel width coefficient (–)		3.59
Channel width exponent (–)		0.35
Channel sediment depth (m)		>1.5

including honey mesquite (*Prosopis glandulosa* Torr.), creosotebush (*Larrea tridentata*), tarbush (*Flourensia cernua*), mariola (*Parthenium incanum*), snakeweed (*Gutierrezia sarothrae*), and several grass species (*Muhlenbergia porteri*, *Pleuraphis mutica*, and *Sporobolus cryptandrus*), with a large percentage of bare soil cover (66%). Vivoni et al. (2014) described the use of UAV imagery and field verification to map species plant cover in the watershed at high resolution (1 m). Here we focus on four main shrubs that occupy large area percentages (mesquite at 6.5%, creosotebush at 5.8%, tarbush at 2.5%, and other shrubs at 14.9%) and for which midday phenocam measurements were available of the green chromatic coordinate (gcc, Luna, 2016; Sonnentag et al., 2012). Additional measurements were obtained of the leaf area index (LAI) and the diurnal pattern of leaf-level stomatal resistance ( $r_s$ ) to complement remotely sensed vegetation data obtained from the Moderate Resolution Imaging Spectroradiometer (MODIS). Field-based and satellite observations were combined to develop a daily series of vegetation parameters, as described in Schreiner-McGraw (2017).



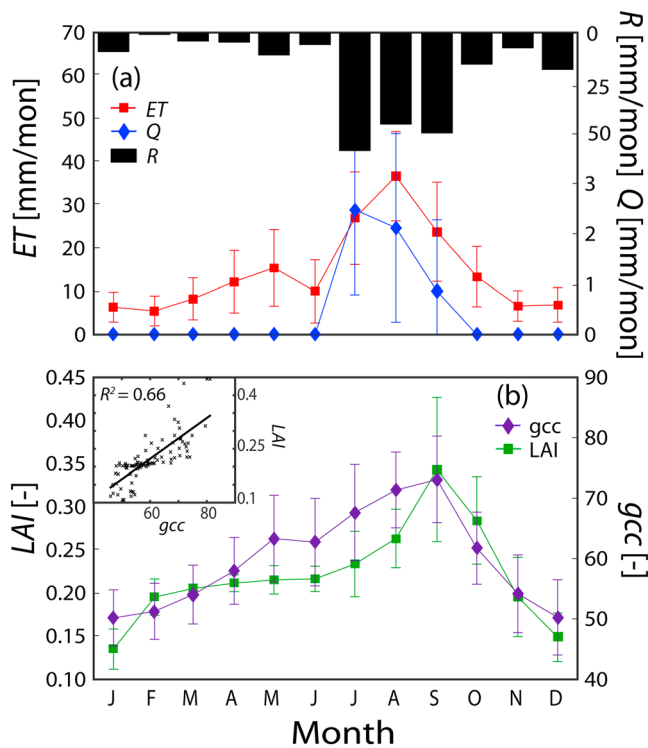


**Figure 2.** Monthly variation of (a) rainfall ( $R$ ), evapotranspiration ( $ET$ ), and runoff ( $Q$ ), and (b) green chromatic coordinate ( $gcc$ ) and leaf area index ( $LAI$ ). Monthly averages and  $\pm 1$  standard deviations (bars) over period 2010–2016. Inset in (b) shows relation between  $gcc$  and  $LAI$ .

## 2.2. Observations From Environmental Sensor Network and Phenocam

Templeton et al. (2014) and Schreiner-McGraw et al. (2016) describe the environmental sensor network in the watershed designed to close the water budget via high temporal resolution (30 min) measurements of rainfall ( $R$ ),  $ET$ , streamflow ( $Q$ ), and soil moisture ( $\theta$ ), as depicted in Figure 1c. This brief description focuses on the data sets used to force, parameterize, or test the hydrologic model over the period 1 July 2010 to 30 September 2016. An EC tower measured meteorological conditions as well as the radiation and energy budgets on a flat surface near the eastern watershed boundary. Incoming solar radiation ( $IS$ ) and net radiation ( $R_n$ ) were measured at 5-m height with a pyranometer (CMP3-L, Campbell Sci.) and a net shortwave and longwave radiometer (CNR2-L, Kipp & Zonen). Latent ( $\lambda ET$ ) and sensible heat flux ( $H$ ) were obtained using a three-dimensional sonic anemometer (CSAT3, Campbell Sci.) and an open-path infrared gas analyzer (LI-7500, LI-COR) installed at 7-m height. Flux corrections followed procedures described in Anderson and Vivoni (2016), and energy balance closure was forced using the Bowen ratio method of Twine et al. (2000) in order to match the approach of Schreiner-McGraw and Vivoni (2017) to estimate percolation and the assumption of energy balance closure in the model physics (Ivanov et al., 2004). As reported by Schreiner-McGraw et al. (2016) and expanded to the full time period for this study, energy balance closure of 83% was obtained. Rainfall measured at four tipping-bucket rain gauges (TE525MM, Texas Electronics) was interpolated by Thiessen polygons to construct the model forcing. Streamflow at the watershed outlet was obtained with a Santa Rita supercritical runoff flume (Smith et al., 1981), a pressure transducer (CS450, Campbell Scientific), and

an in situ calibration (Turnbull et al., 2013). Soil moisture was measured with a network of soil dielectric probes (Hydra Probe, Stevens Water) organized as depth profiles (sensors at 5-, 15-, and 30-cm depths) in north, south, and west facing transects. Following Templeton et al. (2014), aspect and elevation were used to obtain a spatially averaged soil moisture for the watershed ( $\theta_{SN}$ ). Additionally, a cosmic ray neutron sensor (CRNS; CRS-1000b, Hydroinnova) was installed in 2013 to provide spatially averaged soil moisture ( $\theta_{CRNS}$ ).

To illustrate the watershed observations, Figure 2 presents the seasonal cycle of the water balance components ( $R$ ,  $ET$ , and  $Q$ ) along with monthly variations of vegetation conditions ( $gcc$  and  $LAI$ ). During the period 2010–2016, the North American Monsoon (NAM, July–September) accounted for 70% of the annual rainfall and was closely linked to vegetation green-up in the summer. Lagged responses are noted between the peak in summer rainfall (July), the peak  $ET$  (1 month lag in August), and the peak  $LAI$  (2-month lag in September), consistent with prior studies in other ecosystems of the region (e.g., Méndez-Barroso et al., 2014; Vivoni et al., 2008). In contrast, the winter through early summer are generally dry, with  $ET$  exceeding  $R$  ( $ET/R = 1.58$ ), when  $Q$  is 0, an indication that water is being consumed from available storage. In the spring,  $ET$  and phenocam-derived  $gcc$  of the mixed shrubland are influenced by the species-level phenology of creosotebush and mesquite, though these have a limited impact on the ecosystem  $LAI$  (see Figure 2b inset for empirical relation of  $gcc$  and MODIS-based  $LAI$ , validated with site measurements using a ceptometer, Li-COR LAI-2200). Interestingly, the peak  $Q$  at the watershed outlet occurs in July coincident with rainfall, though streamflow amounts are quite low relative to monthly  $R$  and  $ET$ . The lack of a progressive increase in  $Q$  during the NAM, as noted by Robles-Morua et al. (2012), along with the lagged  $ET$  and  $LAI$ , suggests that accumulated soil water does not provide a major control on the observed streamflow. Clearly, modeling the seasonal cycle of the water balance components requires that attention be placed on the type of runoff generation and its loss mechanisms operating in the watershed, as described in the following.

## 2.3. Model Description Including Channel Transmission Losses

Numerical simulations were performed in the watershed using tRIBS, a fully distributed model of hydrologic processes (Ivanov et al., 2004; Vivoni et al., 2007). To make full use of available high-resolution data sets, tRIBS

has a spatially explicit treatment of topography, soil, vegetation, and meteorological conditions and resamples each to the model domain. A watershed is represented by a TIN consisting of elevation, channel, and boundary nodes (Vivoni et al., 2004), which are used to form Voronoi polygons that serve as the computational elements for water and energy balance calculations. For each Voronoi polygon, the model accounts for a range of processes that track the spatiotemporal watershed response, including (1) canopy interception and evaporation; (2) infiltration, soil moisture redistribution, and runoff generation; (3) evaporation from bare soil and transpiration from vegetation; (4) shallow subsurface flow; and (5) overland and channel flow. Recent developments used in this work include a method for ingesting time-variable vegetation parameter values (Vivoni, 2012) and a parallelization method based on subdomain partitioning of the channel network (Vivoni et al., 2011). In previous studies, tRIBS has shown good performance with respect to soil moisture and temperature, ET, and streamflow measurements (e.g., Hawkins et al., 2015; Mahmood & Vivoni, 2011; Méndez-Barroso et al., 2014; Pierini et al., 2014; Xiang et al., 2014).

Given the emphasis of this study, we briefly describe the infiltration, runoff generation, and ET dynamics in the distributed model as applicable for dryland systems with shallow soils. Each Voronoi polygon represents a heterogeneous, sloped soil column above an impermeable layer. A modified version of the Green-Ampt equation for unsaturated flow in layered soils is used to calculate infiltration (Garrote & Bras, 1995; Ivanov et al., 2004). Single infiltration fronts are simulated for each rainfall event and interact with a prestorm moisture profile determined from hydrostatic equilibrium to produce a soil moisture state that affects further infiltration and runoff generation. Soil evaporation and plant transpiration are extracted from available soil moisture according to atmospheric demand, which is estimated by closing the energy balance using the Penman-Monteith equation (Ivanov et al., 2004). In addition to vertical infiltration, tRIBS simulates lateral redistribution in the soil layer based on gradients in surface topography. Surface runoff can be generated on hillslopes as either Hortonian (infiltration-excess) or Dunnian (saturation-excess) runoff when there is a lack of groundwater contributions. Runoff is routed downstream toward the watershed outlet along hillslope and channel segments that are parameterized separately (Ivanov et al., 2004). On hillslopes, bulk transport is assumed to be the dominant factor and the hillslope travel time is calculated as the hillslope path length divided by a velocity dependent on the downstream channel discharge (Garrote & Bras, 1995; Vivoni et al., 2007). In the channel network, a one-dimensional, finite element, kinematic wave approximation is used based on the application of Manning's equation for rectangular cross sections established between channel nodes (see Ivanov, 2002, for details).

To account for channel transmission losses in the watershed, we modified the kinematic wave routing scheme using two methods that differ in their treatment of capillary forces during the initial period of infiltration into channel sediments. The Constant Loss method reduces channel streamflow ( $Q_c$ ) by an amount dependent on the saturated hydraulic conductivity ( $K_{chan}$ ) of channel sediments as (Schoener, 2017) follows:

$$P_{CL} = K_{chan} W_c L_c, \quad (1)$$

where  $P_{CL}$  is the resulting percolation (or transmission) loss and  $W_c$  and  $L_c$  are the channel width and length, respectively. The Transient Loss method accounts for the higher infiltration rates initially observed during the wetting process in dry, ephemeral channels (Blasch et al., 2006) as follows:

$$P_{TL} = \begin{cases} K_{tc} W_c L_c & 0 \leq t \leq \tau \\ K_{chan} W_c L_c & t > \tau \end{cases}, \quad (2)$$

where  $P_{TL}$  is the percolation loss from the method,  $K_{tc}$  is the transient channel hydraulic conductivity,  $t$  is time since streamflow initiation, and  $\tau$  is the length of the transient period.

#### 2.4. Meteorological Forcing, Model Parameterization, and Performance Evaluation

Hydrologic simulations were performed for the mixed shrubland watershed over the study period (6.25 years), divided into two subsets with similar lengths and overall rainfall conditions: (1) a calibration period from 1 July 2010 to 31 December 2013 and (2) a validation period from 1 January 2014 to 30 September 2016. Initial conditions in the model were determined using soil moisture observations on 1 July 2010. Meteorological forcing consisted of 30-min observations of IS, wind speed, air temperature, relative

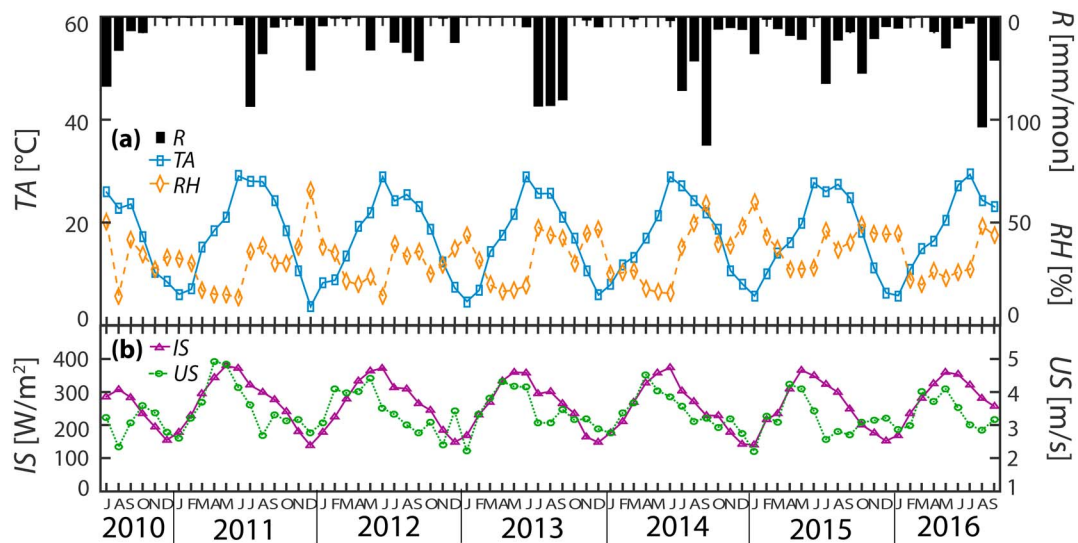


**Figure 3.** Monthly variation of meteorological forcings of (a) rainfall ( $R$ ), air temperature ( $TA$ ), and relative humidity ( $RH$ ) and (b) incoming solar radiation ( $IS$ ) and wind speed ( $US$ ).

humidity, and barometric pressure ( $PA$ ) from the EC tower and applied uniformly to the watershed, while rainfall ( $R$ ) at 30-min resolution was derived through the application of Thiessen polygons to the observations at four sites. We note that aggregation of meteorological data to 30-min resolution suppresses finer-scale variations, which can be important for the short-duration high rainfall intensities at the site (e.g., Templeton et al., 2014; Wainwright, 2006). Other quality-controlled EC observations were used only for model calibration and validation purposes, including net radiation, sensible and latent heat flux, and soil moisture at multiple depths. Gaps in meteorological forcings were filled in with comparable data from the Jornada Soil Climate Analysis Network station located 10 km away (Harms, 2015), while 4 months (August 2010, February 2011, January 2013, and October 2015) was excluded in the model performance evaluation due to gaps in available data. Data gaps consisted of 11% to 13% of the study period for the meteorological forcings, except  $PA$  where instrument failure resulted in a gap for 25% of the time. Figure 3 presents monthly values of the meteorological forcings to the model, highlighting the seasonality of rainfall during the warm season in the Chihuahuan Desert. Air temperature and  $IS$  peak in the late spring ( $29\text{ }^{\circ}\text{C}$  and  $355\text{ W/m}^2$ , respectively) and decrease to some extent during the NAM ( $27\text{ }^{\circ}\text{C}$  and  $350\text{ W/m}^2$ ) due to sporadic cloud cover. The winter season typically has low rainfall amounts and air temperatures above freezing, such that cold-season processes (Rinehart et al., 2008) are not considered here.

The model domain for the watershed, consisting of the TIN and its associated Voronoi polygons, was derived from the DEM using the methods of Vivoni et al. (2004). By retaining all pixels in the DEM, the Voronoi polygons are approximately squares at 1-m spatial resolution, except near the channel network and watershed boundary where the linear features are preserved. With this approach, terrain properties, such as slope, aspect, and curvature, from the original DEM are transferred to the model domain without a loss of information, as depicted in Figure 4a. Similarly, Voronoi polygons were assigned a land cover class based on the UAV-based image classification into five types: mesquite, creosotebush, tarbush, grass, and bare soil (Figure 4b) and used to specify vegetation parameters. Other shrubs were classified as tarbush (total of 17.4% in area), due to similar phenology and lack of species-specific data. Figure 5 shows examples for three time-variable vegetation parameters—vegetation fraction ( $v_f$ ), optical transmission coefficient ( $k_t$ ), and minimum canopy stomatal resistance ( $r_s$ )—derived from the phenocam and MODIS data, following Méndez-Barroso et al. (2014). As in Pierini et al. (2014), the land cover classes were used to specify soil properties as well, under the assumption that local variations occur in litter, organic matter, and eolian deposition due to differences in plant cover (Howes, 1999; Mueller et al., 2007; Parsons et al., 2003). While soil analyses were performed by Anderson and Vivoni (2016) at 25 locations around the EC tower, a high-resolution representation of soil texture, gravel content, or depth to the calcium carbonate horizon are not available at present. Thus, we utilized

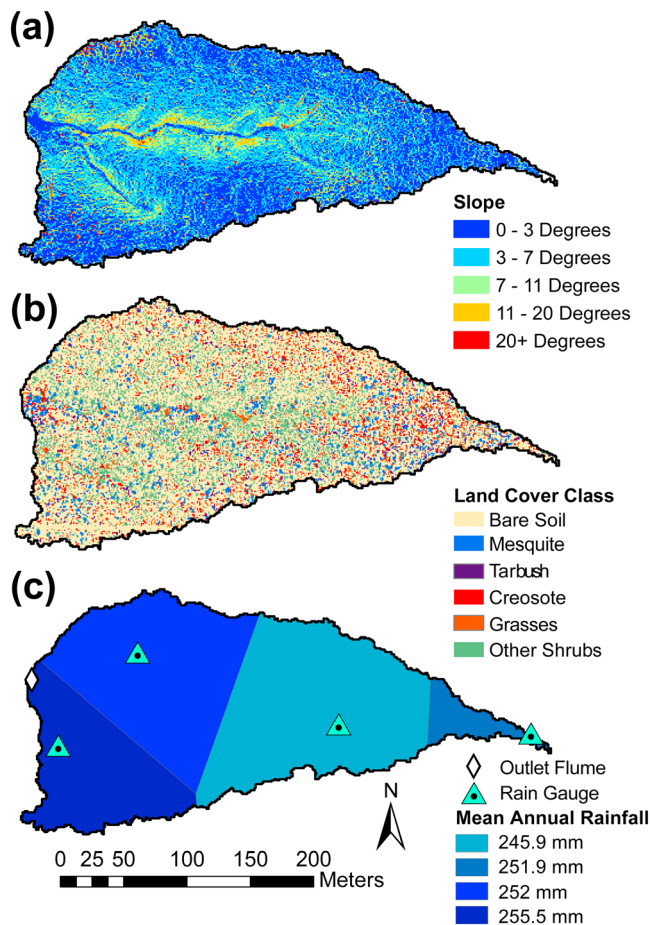


**Figure 4.** Spatial variation of (a) slope, (b) land cover class, and (c) mean annual rainfall based on Thiessen polygons of four rain gauge sites.

a spatially uniform soil depth of 50 cm and treated the calcium carbonate layer as an impermeable lower boundary in the model. This is consistent with soil moisture data at the EC tower indicating that infiltration fronts did not penetrate to 50 cm over the study period.

Initial model parameters were based on a combination of field sampling efforts, prior studies with the model (Méndez-Barroso et al., 2014; Pierini et al., 2014; Vivoni et al., 2014) and a literature review for the soils and vegetation species in the watershed (e.g., Dugas et al., 1996; Duniway et al., 2010; Mueller et al., 2007; Rawls et al., 1983). Table 2 presents the soil and vegetation parameter values obtained for the land cover classes, as well as the channel parameters, and their respective sources. Additional information on parameters is available in Ivanov et al. (2004) and Vivoni et al. (2007). Manual calibration was performed for a subset of parameters to match observed conditions (shown in Table 2 with labels 5, 6, and 7), including (1) energy balance and its partitioning at the EC tower, (2) soil moisture dynamics at individual sites and averaged in the watershed, (3) hillslope infiltration during rainfall events, and (4) monthly percolation estimates from the watershed water balance. Simulated surface soil moisture over the top 10 cm ( $\theta_{sur}$ ) was compared to 5-cm depth observations, while root zone soil moisture over the top 50 cm ( $\theta_{root}$ ) was compared to a weighted average of measurements at 5, 15, and 30 cm. Similarly, the simulated soil moisture in the CRNS footprint ( $\theta_{CRNS}$ ) is weighted according to the time-variable measurement depth of the sensor (Schreiner-McGraw et al., 2016). Outlet streamflow is dependent on channel percolation being simulated correctly and thus is considered as a validation that watershed processes are accounted for correctly. Independent, split-sample model testing was performed over 1 January 2014 to 30 September 2016. By calibrating and validating the model with the full set of observations simultaneously, we ensure a consistent representation of the simulated watershed response with the objective of reproducing the main features of the rainfall and runoff response described by Schreiner-McGraw and Vivoni (2017). Model performance was assessed using the mean absolute error (MAE), correlation coefficient (CC), and bias (B) as goodness of fit metrics for the aforementioned observations at daily and monthly resolutions, as described in Pierini et al., (2014, their Appendix A).

### 2.5. Numerical Experiments and Modeling Scenarios

We performed numerical experiments to assess the sensitivity of the watershed response to the method employed for channel transmission losses (*Constant Loss*,  $P_{CL}$ , and *Transient Loss*,  $P_{TL}$ ) and compared these results to the original model formulation (Ivanov et al., 2004) without channel losses (labeled *No Percolation*). In these experiments, the Transient Loss method constitutes the setup that underwent a full calibration and validation, whereas the channel properties were not calibrated for the No Percolation and Constant Loss cases. Subsequently, we constructed a set of modeling scenarios to explore the impact of hillslope and channel properties on runoff generation and percolation mechanisms at the monthly scale. The scenarios sample individual and joint variations in the saturated hydraulic conductivity of hillslope ( $K_{hill}$ ) and channel ( $K_{chan}$ ) areas in the watershed based on changes to the parameter values shown in Table 2 within plausible ranges (e.g., Goodrich et al., 1997; Keppel & Renard, 1962; Tromble et al., 1974). Simulations that modify hillslope infiltration properties change the weighted average of all land covers in the watershed while preserving the relative relations between the saturated hydraulic conductivity of different classes (e.g., the bare soil patches remain lower than vegetated areas by the same relative amount). We also explored the comparative importance of hillslope and channel properties on the simulated percolation losses and their impact on the outlet streamflow yield. All modeling scenarios received the same initialization had a constant set of meteorological forcing and time-variable vegetation properties and spanned the full study period.



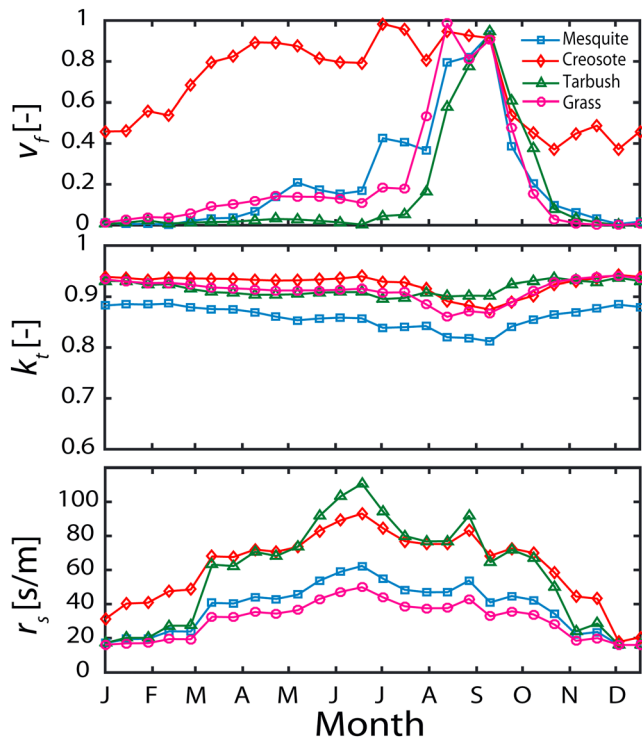


**Figure 5.** Biweekly variation of vegetation fraction ( $v_f$ ), optical transmission coefficient ( $k_t$ ), and minimum canopy stomatal resistance ( $r_s$ ) for different species.

presentation is likely due to springtime water uptake by mesquite from deeper soil layers, including calcium carbonate horizons (e.g., Duniway et al., 2010). While mesquite phenology is captured in the model (Figure 5), dry soils prevent simulated transpiration losses, as noted in other ecosystems of the region (e.g., Scott, 2010). As a result, modeling improvements are needed in specifying how mesquites extract water from deep, calcareous layers that serve as a long-term storage of hillslope infiltration losses.

### 3. Results

#### 3.1. Evaluation of Simulated Water and Energy Dynamics on Hillslopes

Simulated water and energy states and fluxes in the arid piedmont watershed were compared to available observations over the calibration, validation, and full study periods. Table 3 shows the metrics obtained for daily and monthly values, where CC and B close to 1 and low MAE indicate satisfactory model performance for energy fluxes ( $R_r$ ,  $H$ , and  $\lambda ET$ ), soil moisture states ( $\theta_{sur}$ ,  $\theta_{root}$ , and  $\theta_{CRNS}$ ), and monthly percolation from the two methods ( $P_{CL}$  and  $P_{TL}$ ). For instance, the simulated energy fluxes exhibit a good correspondence to the observations with a high CC ( $>0.93$ ), B near unity (from 0.88 to 1.02), and MAE less than  $10.76 \text{ W/m}^2$  for monthly values across the three periods. Figure 6 illustrates the model performance with respect to the seasonal cycle of the energy fluxes as averaged monthly conditions (symbols) and interannual variations ( $\pm 1$  standard deviation as error bars) over the full study period. The effect of the rainy season during the NAM is clearly noted (July to September) by a decrease in  $H$  and an increase in  $\lambda ET$  in response to available soil water and a small decrease in  $R_r$  due to sporadic cloud cover. Overall, the hydrologic model adequately captures monthly variations in the energy fluxes measured at the EC tower when accounting for the fractions of bare soil and vegetation in the footprint (Anderson & Vivoni, 2016). Nevertheless, the observed  $\lambda ET$  is underestimated during the spring by an average of  $9.25 \text{ W/m}^2$ , though differences are within the standard deviation for all months. This misre-

**Table 2**  
Static Model Parameters<sup>a</sup>

Parameter	Variable (unit)	Land surface classification						Source
		Bare soil	Mesquite	Creosote	Tarbush	Other shrub	Grass	
A	Area (%)	66	6.5	5.8	2.5	14.9	4.3	1
$K_{hill}$	Hillslope hydraulic conductivity (mm/hr)	1.1	6	3.3	3.3	3.3	3.3	2 and 5
$n$	Soil porosity ( $\text{m}^3/\text{m}^3$ )	0.5	0.5	0.5	0.5	0.5	0.5	3 and 4
$\theta_s$	Saturated soil moisture ( $\text{m}^3/\text{m}^3$ )	0.23	0.23	0.23	0.23	0.23	0.23	3 and 4
$\theta_r$	Residual soil moisture ( $\text{m}^3/\text{m}^3$ )	0.02	0.02	0.02	0.02	0.02	0.02	3 and 4
$m$	Pore size distribution index ( $\text{m}^3/\text{m}^3$ )	0.6	0.6	0.6	0.6	0.6	0.6	5
$\psi_b$	Air entry bubbling pressure (mm)	-0.0001	-0.0001	-0.0001	-0.0001	-0.0001	-0.0001	5
$A_s$	Saturated anisotropy ratio (dimensionless)	1	1	1	1	1	1	5
$A_u$	Unsaturated anisotropy ratio (dimensionless)	50	50	50	50	50	50	5
$k_s$	Soil heat conductivity (J/msK)	5	5	5	5	5	5	6
$C_s$	Soil heat capacity ( $\text{J/m}^3\text{K}$ )	200,000	200,000	200,000	200,000	200,000	200,000	6
$Z_r$	Soil depth (m)	0.5	0.5	0.5	0.5	0.5	0.5	3
$h$	Vegetation height (m)	0	1.5	1	1	1	0.3	3
$K_{chan}$	Channel hydraulic conductivity (mm/hr and m/day)	663 and 0.028						4
$k_{tc}$	Channel transient hydraulic conductivity (mm/hr and m/day)	46,410 and 1.934						7
$\tau$	Transient time (hr)	1						7

<sup>a</sup>Sources for time-invariant model parameters are as follows: 1, unmanned aerial vehicle image from Templeton et al. (2014); 2, Mueller et al. (2007); 3, Schreiner-McGraw et al. (2016); 4, average of observations by Schreiner-McGraw (2017) at seven locations in main channel in June 2017 using a double ring infiltrometer; 5, calibration on the basis of soil moisture data comparison; 6, calibration on the basis of soil temperature data comparison; and 7, calibration on the basis of percolation data comparison.

Values	Variable	Calibration (2010–2013)			Validation (2014–2016)			Full period (2010–2016)		
		CC	B	MAE	CC	B	MAE	CC	B	MAE
Daily values	$R_n$ ( $W/m^2$ )	0.98	0.94	6.94	0.98	0.92	15.11	0.98	0.90	12.14
	$H$ ( $W/m^2$ )	0.93	1.17	32.15	0.93	1.06	11.43	0.93	1.11	21.21
	$\lambda ET$ ( $W/m^2$ )	0.90	0.92	16.23	0.82	0.90	19.65	0.85	0.87	18.10
	$\theta_{sur}$ ( $m^3/m^3$ )	0.85	0.86	0.00	0.72	0.86	0.00	0.77	0.86	0.00
	$\theta_{root}$ ( $m^3/m^3$ )	0.65	0.65	0.01	0.65	0.65	0.01	0.65	0.67	0.02
	$\theta_{CRNS}$ ( $m^3/m^3$ )	0.70	0.72	0.02	0.66	0.66	0.01	0.68	0.69	0.02
Monthly values	$R_n$ ( $W/m^2$ )	1.00	0.95	5.84	1.00	0.91	10.76	1.00	0.92	8.36
	$H$ ( $W/m^2$ )	0.98	1.02	5.89	0.99	0.98	3.92	0.99	1.00	0.53
	$\lambda ET$ ( $W/m^2$ )	0.93	0.88	2.28	0.93	0.92	1.60	0.94	0.96	0.75
	$\theta_{sur}$ ( $m^3/m^3$ )	0.93	1.03	0.00	0.70	0.93	0.02	0.80	0.96	0.01
	$\theta_{root}$ ( $m^3/m^3$ )	0.91	0.79	0.01	0.57	0.97	0.01	0.70	0.88	0.01
	$\theta_{CRNS}$ ( $m^3/m^3$ )	0.75	0.78	0.00	0.54	0.61	0.01	0.69	0.69	0.01
	$P_{CL}$ (mm)	0.88	0.25	4.24	0.68	0.28	3.90	0.76	0.26	4.09
	$P_{TL}$ (mm)	0.87	0.99	0.07	0.78	0.94	0.34	0.81	0.99	0.19

Figure 7 presents a comparison of the observed and simulated soil moisture states and ET at a daily temporal resolution for the full study period. The observed surface ( $\theta_{sur}$ ) and root zone ( $\theta_{root}$ ) soil moisture values are spatial averages across the sensor network and compared to averaged conditions of the corresponding Voronoi polygons (15 sites, Figure 1c). For a subset of time (8 January 2013 to 31 December 2015), comparisons are also made of  $\theta_{CRNS}$ , which take into account the spatial aggregation of soil moisture occurring in the sensor footprint. Model performance is adequate with respect to spatially averaged soil moisture dynamics at the sensor network and watershed scales, with better goodness of fit metrics for monthly values and shallower depths (Table 3).

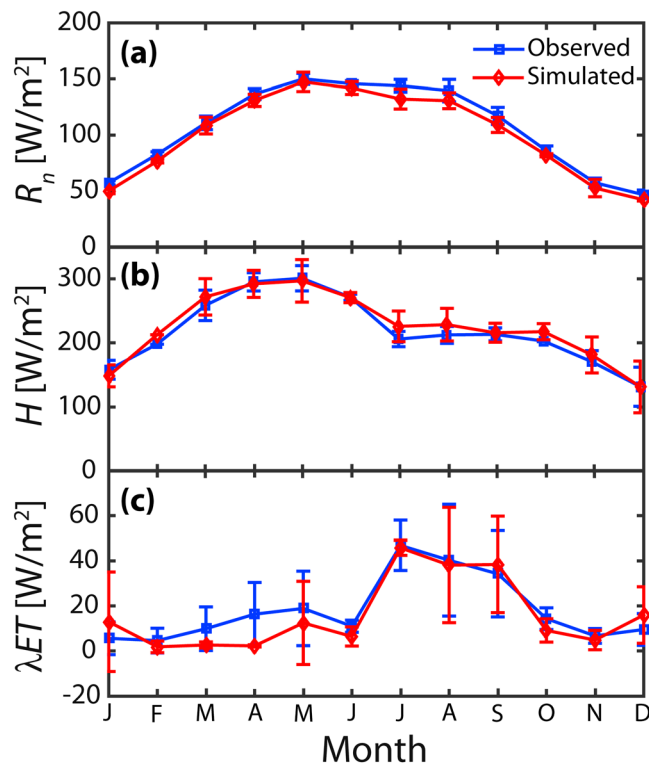


**Figure 6.** Monthly variation of observed and simulated surface energy fluxes over period 2010–2016: (a) net radiation ( $R_n$ ), (b) sensible heat flux ( $H$ ), and (c) latent heat flux ( $\lambda ET$ ). Symbols indicate averages and the bars represent  $\pm 1$  standard deviations.

Although the effects of infiltration fronts on soil moisture increases are simulated well, there are limitations in capturing the recession characteristics (i.e., model overestimates the soil water losses), in particular, for deeper layers and in the winter periods (i.e., progressively lower Bias). Overall, simulated ET matches daily and monthly observations well ( $\lambda ET$  with  $CC > 0.85$ ,  $B$  within  $\pm 0.12$  of unity,  $MAE < 20 W/m^2$ , Table 3). As noted previously, spring ET is underestimated, while wintertime ET is overestimated (December–January, Figure 6), which leads to lower  $\theta_{sur}$  and  $\theta_{root}$  in the simulations for the winter and a lack of accumulation of soil water in the spring. This is attributed to an enhancement of shallow soil evaporation in the model when the majority of the vegetation species do not have leaves in the winter (Figure 5).

Despite these discrepancies, the simulation of shallow soil moisture is encouraging, in particular, during the NAM when hillslope runoff production is more prevalent. Given the tight link between  $\theta_{sur}$  and infiltration-excess runoff (Beven, 2012), we compared the observed and simulated infiltration front depths ( $N_f$ ) after 18 storm events during the study period (Figure 8). Storms were selected to have a single infiltration front (i.e., individual pulses) and for moderate to low antecedent conditions ( $\theta_{sur} < 0.1 m^3/m^3$ ) to facilitate obtaining the maximum infiltration depth occurring over 3 days after each storm event. Average values of  $N_f$  were obtained from all sensor profiles and corresponding Voronoi polygons. The majority of the observed infiltration fronts were contained within the top 150 mm of soil due to the quantized nature of the sensor profiles (5-, 15-, and 30-cm depths). A logarithmic regression obtained between rainfall event depth ( $R$  in millimeter) and infiltration front depth ( $N_f = 107 \ln(R) - 174$  in millimeter) from the sensor data (labeled *Observed Regression*) was found to capture the simulated value of  $N_f$  well, with

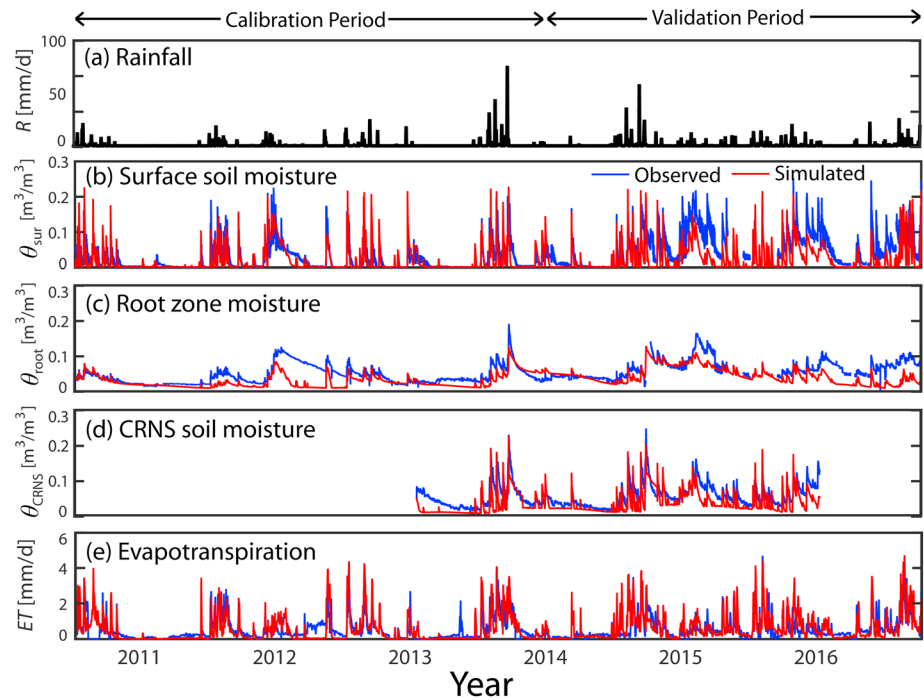


**Figure 7.** Observed and simulated daily variables: (a) rainfall forcing, and spatially averaged soil moisture for the (b) surface, (c) root zone, (d) cosmic ray neutron sensor depths, and (e) evapotranspiration. The calibration and validation period extents are indicated. SEE = standard errors of estimates.

similar coefficients of determination ( $R^2$ ) and standard errors of estimates (SEE). Thus, the model represents well the depths of soil water infiltration across a range of rainfall event sizes, suggesting that infiltration-excess runoff on hillslopes is generated adequately during storms.

### 3.2. Percolation and Its Controls on Outlet Streamflow

Model simulations of percolation losses from two methods (Constant Loss and Transient Loss) are compared to estimates from the watershed water balance in Figure 9 as monthly and cumulative values, while Table 3

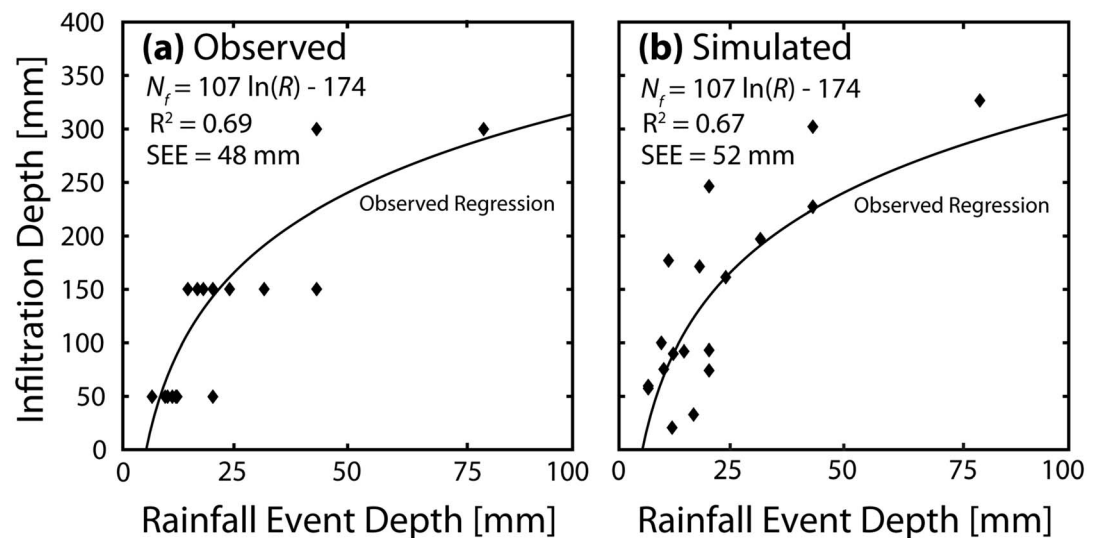


**Figure 8.** Observed (a) and simulated (b) soil infiltration depths ( $N_f$ ) for different rainfall event depths ( $R$ ). Observed regression line obtained from (a) was applied to the simulations in (b). Coefficients of determination ( $R^2$ ) and standard error of estimates shown. ET = evapotranspiration; CRNS = cosmic ray neutron sensor.

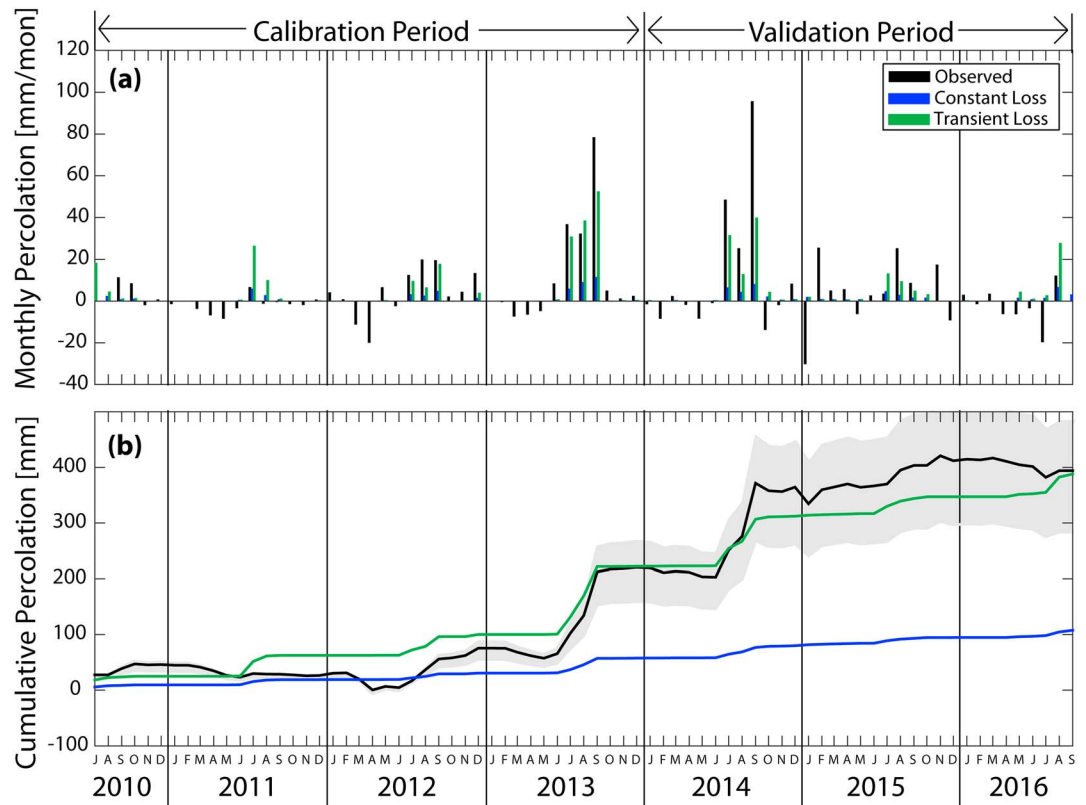


**Figure 9.** (a) Monthly and (b) cumulative percolation from watershed water balance observations (labeled *Observed*) and simulations using the Constant Loss and Transient Loss methods. The calibration and validation period extents are indicated. Note that the simulations have monthly percolation values that are equal to or greater than 0.

provides performance metrics. Following Schreiner-McGraw and Vivoni (2017, their Table 2), we have accounted for potential sources of uncertainty in the percolation estimates through a shaded envelope. Since monthly residuals of the water balance can be either positive or negative (Schreiner-McGraw & Vivoni, 2017), we limit comparisons to periods of positive values linked to percolation or channel transmission losses. Clearly, the Constant Loss ( $P_{CL}$ ) approach significantly underestimates the observed values, though it

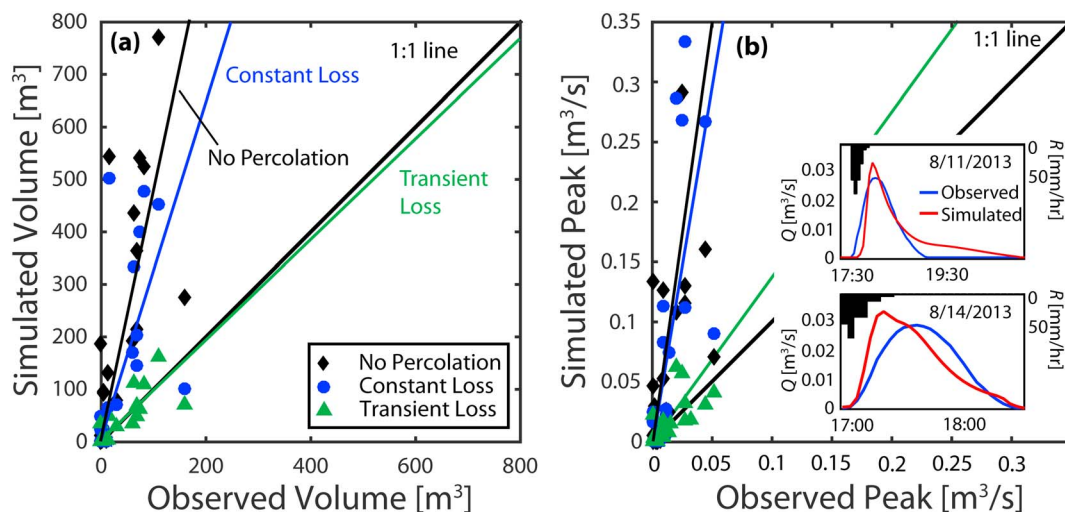


**Figure 10.** Scatterplots of observed and simulated event streamflow metrics: (a) volume and (b) peak discharge, with linear fits for No Percolation, Constant Loss, and Transient Loss methods. Insets in (b) compare simulated and observed outlet hydrographs on 11 and 14 August 2013 for the Transient Loss method.



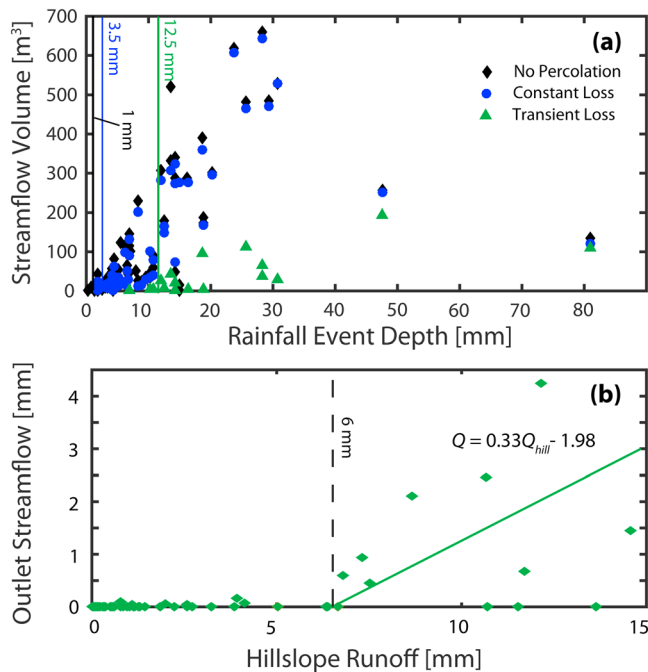


**Figure 11.** (a) Relation of outlet streamflow volume and rainfall event depth for the No Percolation, Constant Loss, and Transient Loss approaches, with vertical lines indicating minimum rainfall required for streamflow. (b) Relation of outlet streamflow ( $Q$ ) and hillslope runoff ( $Q_{hill}$ ) depths for the Transient Loss method illustrating threshold in streamflow response as dashed line.

performs better than the original model formulation (No Percolation, not shown). By relying only on measured values of channel saturated hydraulic conductivity ( $K_{chan}$ , Table 2),  $P_{CL}$  yields a total of 108 mm of percolation loss during the study period for an underestimation Bias (B) of 0.26. In contrast, the Transient Loss ( $P_{TL}$ ) method, which allows higher values of initial infiltration into channel sediments due to capillary forces, yields percolation losses consistent with the observations for a total of 388 mm ( $B = 0.99$  for full study period). To achieve this, the transient value of channel hydraulic conductivity ( $K_{tc}$ ) and transient time ( $\tau$ ) were calibrated to  $70K_{chan}$  and 1 hr, respectively, consistent with observations by Blasch et al. (2006). Note that the majority of percolation losses during the study period occurred during the NAM in 2013 and 2014, though  $P_{TL}$  underestimates the observations for September of each year. Overall, however, the Transient Loss method for channel transmission losses matches well the conceptual model of Schreiner-McGraw and Vivoni (2017) derived from the environmental sensor network. It should be noted, however, that several sources of modeling uncertainty in  $P_{CL}$  and  $P_{TL}$  (e.g., parameter values and meteorological forcing) have not been accounted for, as performed in the observations.

Figure 10 presents scatterplots of observed and simulated outlet streamflow metrics, namely, the streamflow volume and peak discharge, obtained from the three percolation methods. To correctly capture these metrics across all events (26 runoff occurrences during full study period), hillslope runoff production and channel transmission losses both need to be properly simulated. For the No Percolation approach, the streamflow volume and peak discharge values are considerably overestimated ( $B = 4.55$ ,  $SEE = 240 \text{ m}^3$ , and  $B = 3.89$ ,  $SEE = 0.076 \text{ m}^3/\text{s}$ , respectively).

Additionally, when no percolation is assumed, 155 small events that are not present in the observed record are simulated. Similarly, for the Constant Loss approach, the model overestimates streamflow volume and peak discharge values ( $B = 3.12$  and  $B = 5.11$ , respectively), though the number of small events that are not observed is reduced to 76. Clearly, the Transient Loss method exhibits the best performance with respect to streamflow volume and peak discharge ( $B = 0.97$ ,  $SEE = 44 \text{ m}^3$ , and  $B = 1.03$ ,  $SEE = 0.019 \text{ m}^3/\text{s}$ ) and results in 25 simulated events as compared to the 26 runoff occurrences in the observations. To illustrate this point, the insets in Figure 10b present comparisons of observed and simulated outlet streamflow hydrographs for two NAM runoff events in 2013 (11 and 14 August) that vary in terms of their antecedent wetness ( $\theta_{SN} = 0.09$  and  $0.17 \text{ m}^3/\text{m}^3$ , respectively). The high temporal resolution hydrographs are responses to events of similar magnitudes (15.7 and 16.5 mm in 30 min) with peak timing at the outlet shortly after the rainfall peak. Since calibration was not performed for individual events, an excellent correspondence is noted between observed and simulated hydrographs using the Transient Loss method. Furthermore, the simulations are sensitive to the antecedent wetness conditions, as expected, with a lower time lag between the rainfall centroid and peak discharge in the wetter case (3.75 min for 14 August as compared to 7.5 min for 11 August), indicating the important role of hillslope runoff production on the outlet streamflow.

To further diagnose the model response, Figure 11 shows relations among rainfall event sizes, hillslope runoff amounts, and streamflow volumes. Over the full study period, 184 storm events generated hillslope runoff that reached the channel network, with most of these having small depths ( $<10$  mm). Upon reaching the channels, the amounts of percolation loss and the streamflow exiting the watershed depend on the selected method. As channel percolation losses increase, the minimum rainfall event depth required to generate streamflow varies from 1 mm (No Percolation) to 3.5 mm (Constant Loss) and 12.5 mm (Transient Loss), as shown in Figure 11a. After each of these rainfall thresholds is exceeded, an approximately linear increase in streamflow volume at the outlet is noted for higher rainfall depths in each method. This indicates that streamflow yield from the watershed becomes proportional to rainfall event size once an initial amount of channel losses occur. Furthermore, the underlying mechanism responsible for this proportional response is the overland hillslope runoff production, as noted in Figure 11b for the Transient Loss method. A threshold

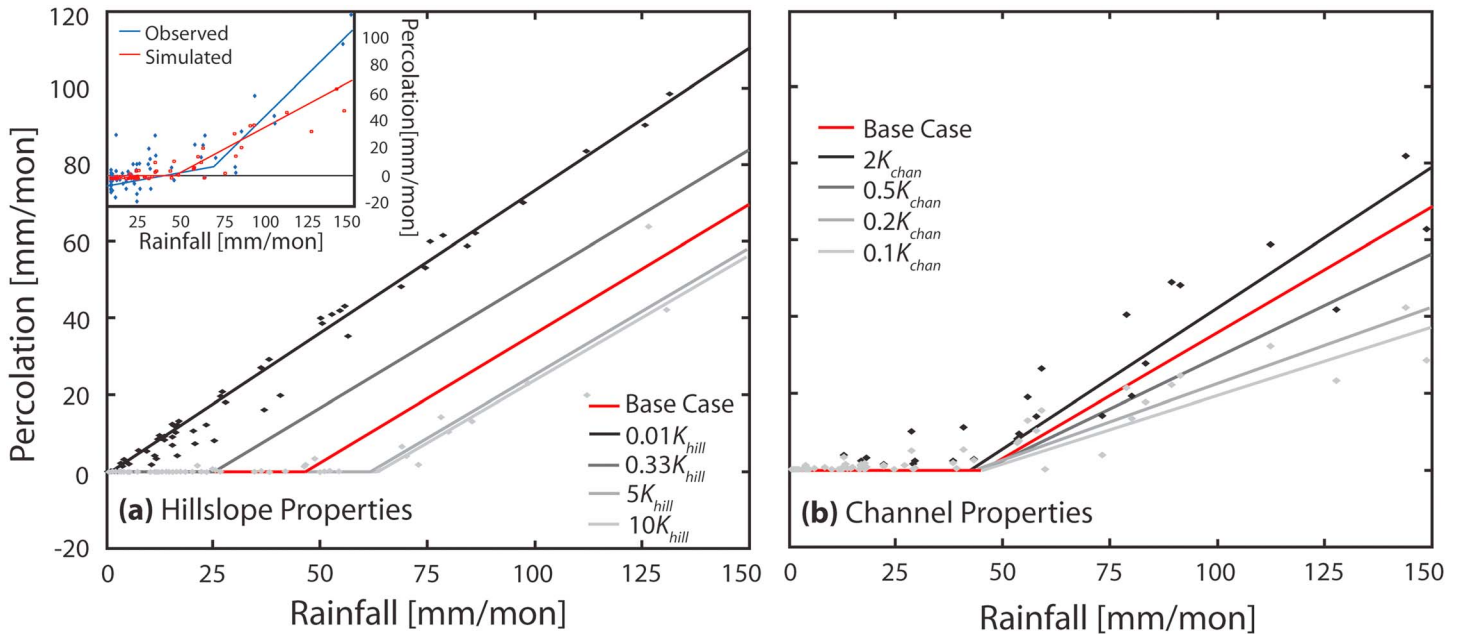


**Figure 12.** Piecewise linear relations between monthly percolation and rainfall for varying (a) hillslope and (b) channel properties. Points are shown for two cases only; others are omitted for clarity. Inset in (a) compares relationships for observed and simulated (Base Case) conditions.

of 6 mm of hillslope runoff is identified below which channels in the watershed are able to absorb all of the overland flow before it reaches the outlet. For larger events, an increase is noted in the outlet streamflow, which can be approximated as a weak linear function ( $Q = 0.33Q_{hill} - 1.98$ ,  $R^2 = 0.13$ ). While the majority of the percolation losses occur during large rainfall events, 40% of the simulated percolation results from small rainfall events that are absorbed in the channel network before reaching the outlet.

### 3.3. Effects of Hillslope and Channel Properties on Percolation

Given the consistent model performance, we explored the effects of hillslope and channel properties on percolation losses through a set of modeling scenarios. Figure 12a presents the effects of hillslope infiltration ( $K_{hill}$ ) on the relation between monthly percolation and rainfall for four scenarios ( $0.01K_{hill}$ ,  $0.33K_{hill}$ ,  $5K_{hill}$ , and  $10K_{hill}$ ) and the calibrated model ( $K_{hill}$ , labeled *Base Case*) whose performance is shown in the inset relative to the estimates of Schreiner-McGraw and Vivoni (2017). In all cases, a piecewise linear relation is used to approximate the relations between  $P$  and  $R$ . The range of tested hillslope infiltration values represents field conditions varying from desert pavements ( $0.01K_{hill}$ , Young et al., 2004) to soils with eolian sand deposits ( $10K_{hill}$ , Monger, 2006). When  $K_{hill}$  is reduced (increased), a lower (higher) rainfall threshold is required to activate channel transmission losses. Nonetheless, the slope of the relation between percolation and rainfall after the threshold is unaltered for the different values of  $K_{hill}$ . As a result, the infiltration capacity of hillslope soils

**Table 4**  
Annual Average Water Balance Terms for Modeling Scenarios

Properties	Scenario	$R$ (mm/year)	ET (mm/year)	$P$ (mm/year)	$Q$ (mm/year)	$Z_r$ ( $\Delta\theta_{root}/\Delta t$ ) (mm/year)	$P/R$	$Q/R$
Hillslope properties	Base case	255	185	65	7	-2	0.25	0.03
	$0.01K_{hill}$	255	46	192	19	-3	0.75	0.07
	$0.33K_{hill}$	255	147	98	12	-2	0.38	0.05
	$5K_{hill}$	255	204	50	1	-1	0.20	0.01
	$10K_{hill}$	255	206	48	1	-1	0.19	0.01
Channel properties	$0.1K_{chan}$	255	185	40	33	-2	0.16	0.13
	$0.2K_{chan}$	255	185	49	23	-2	0.19	0.09
	$0.5K_{chan}$	255	185	59	13	-2	0.23	0.05
	$2K_{chan}$	255	185	68	4	-3	0.27	0.02

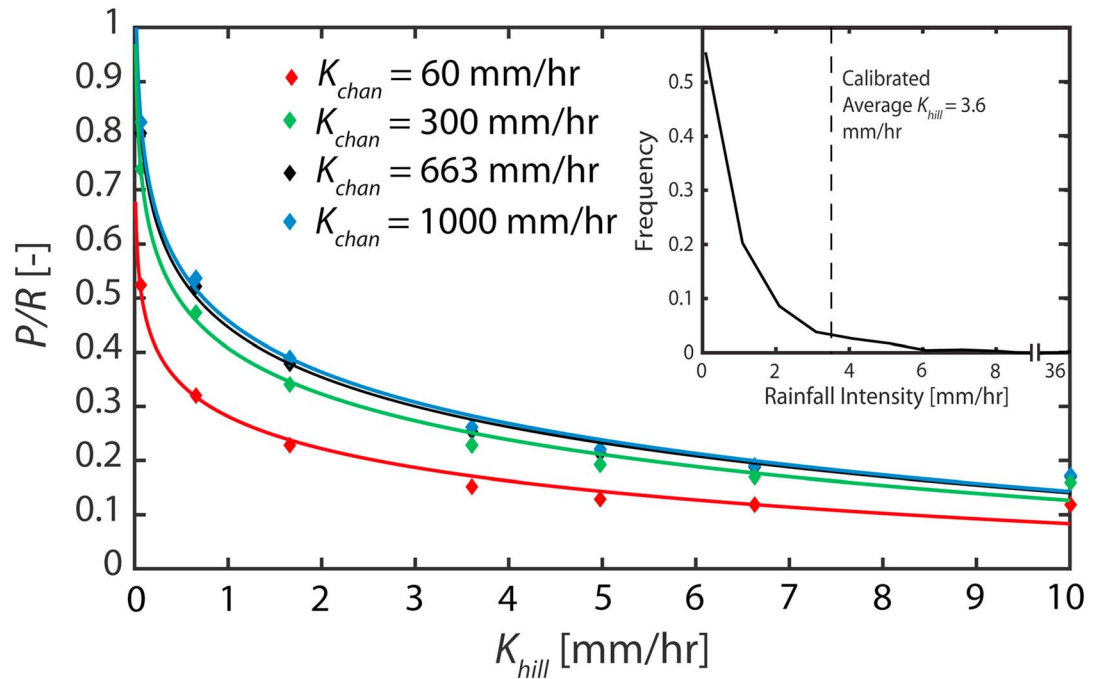


**Figure 13.** Relations between the monthly percolation to rainfall ( $P/R$ ) ratio and hillslope hydraulic conductivity ( $K_{hill}$ ) for a variety of channel hydraulic conductivity ( $K_{chan}$ ) values. Inset shows the frequency distribution of observed rainfall intensity in relation to the calibrated value of  $K_{hill}$ .

primarily affects percolation losses by reducing or augmenting hillslope runoff delivered to channels. In addition, large variations are noted in the water balance partitioning among the cases (Table 4), with the higher  $P/R$  occurring under lower  $K_{hill}$  also linked to lower ET due to less soil infiltration. In a similar manner, Figure 12b shows the sensitivity of the relation of monthly  $P$  and  $R$  to channel infiltration ( $0.1K_{chan}$ ,  $0.2K_{chan}$ ,  $0.5K_{chan}$ , and  $2K_{chan}$ ), including the calibrated model ( $K_{chan}$ , Base Case). In contrast to the hillslope effects, changes in  $K_{chan}$  affect the slope of the relation between percolation and rainfall but have a minimal impact on the rainfall

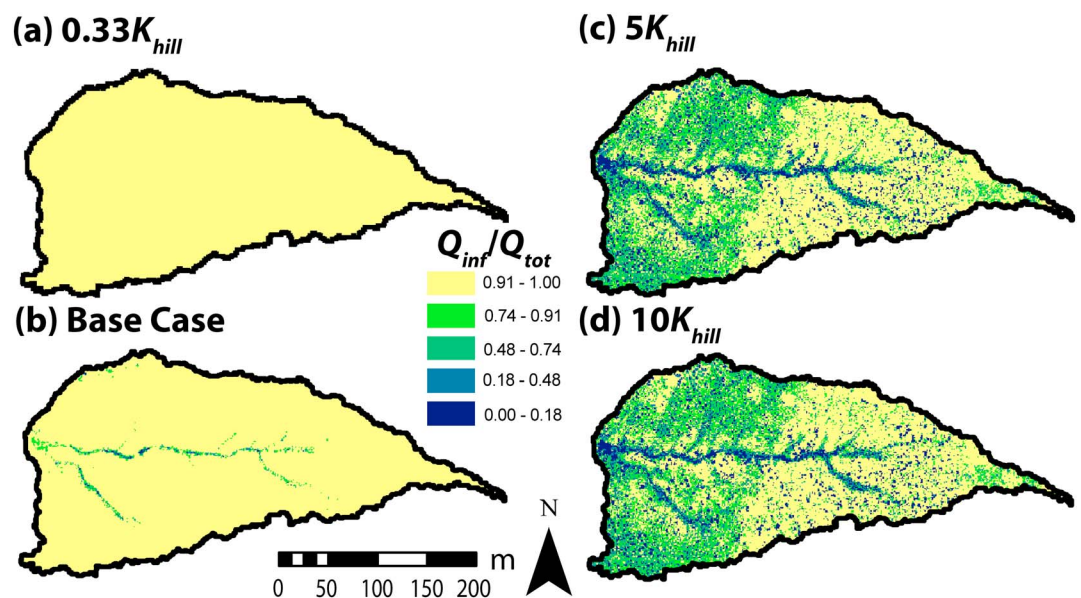


**Figure 14.** Spatial distribution of the simulated ratio of infiltration excess to total runoff ( $Q_{inf}/Q_{tot}$ ) for (a)  $0.33K_{hill}$ , (b)  $K_{hill}$  (Base Case), (c)  $5K_{hill}$ , and (d)  $10K_{hill}$  scenarios.

threshold at which channel losses begin. As expected, lower  $K_{\text{chan}}$  leads to lower  $P$  and higher  $Q$ , and vice versa. Furthermore, variations in the water balance components among the cases are limited to percolation and streamflow (Table 4), without an impact on the simulated ET that is determined nearly exclusively by hillslope properties.

Clearly, both hillslope and channel properties play important but varying roles in the partitioning of the watershed water balance. We assessed the relative importance of  $K_{\text{hill}}$  and  $K_{\text{chan}}$  on  $P/R$  in Figure 13 by simultaneously varying these properties. For reference, the Base Case is characterized by  $K_{\text{hill}} = 3.6$  mm/hr and  $K_{\text{chan}} = 663$  mm/hr using the Transient Loss method. Note that the inset shows the relation between the calibrated  $K_{\text{hill}}$  and the distribution of rainfall intensities, which identifies the events that generate infiltration-excess runoff. Changes in  $K_{\text{hill}}$  lead to a logarithmic variation of  $P/R$ , with large percolation losses ( $P/R$  approaching 1) when hillslope infiltration is reduced ( $K_{\text{hill}}$  approaching 0). As  $K_{\text{hill}}$  increases, soil infiltration and subsequent ET become more important and the rainfall threshold required to produce percolation increases. Over the range of tested values, variations in  $K_{\text{hill}}$  result in changes of  $P/R$  from 0.12 to 0.52 (for  $K_{\text{chan}} = 60$  mm/hr) and from 0.17 to 0.82 (for  $K_{\text{chan}} = 1,000$  mm/hr). Thus, while there is sensitivity to channel infiltration, the range of  $K_{\text{chan}}$  leads to proportionally smaller variations in  $P/R$ . This is attributed to the strong control exerted by the transient period ( $\tau = 1$  hr) and its increased hydraulic conductivity on percolation losses during short-duration events. However, if  $K_{\text{chan}}$  is reduced to 60 mm/hr,  $P/R$  is decreased by  $\sim 50\%$  across a wide range of  $K_{\text{hill}}$ , suggesting that the presence of calcium carbonate layers in channels (Lekach et al., 1998) would have a large impact on streamflow yield. Overall, the sensitivity of the Base Case to changes in  $K_{\text{hill}}$  and  $K_{\text{chan}}$  suggests that small changes in hillslope infiltration ( $\sim 1$  to 2 mm/hr) have larger consequences on  $P/R$  ( $\pm \sim 33\%$  difference) than more drastic changes in channel infiltration (300 to 400 mm/hr leading to  $\pm \sim 5\%$  difference in  $P/R$ ). This is consistent with the high ratio of hillslope to channel surface area of 67 (Table 1). As a result, the partitioning of precipitation into infiltration and runoff within hillslopes is more sensitive than the partitioning of flow into percolation and streamflow for the range of infiltration values representative of site conditions.

To further explore the impact of hillslope infiltration on runoff production, Figure 14 displays the spatial variability of the fraction of total runoff attributed to the infiltration-excess mechanism ( $Q_{\text{inf}}/Q_{\text{tot}}$ ). For cases with  $K_{\text{hill}}$  lower than the calibrated conditions (e.g., desert pavement surfaces), infiltration-excess runoff is the dominant mechanism throughout the watershed ( $Q_{\text{inf}}/Q_{\text{tot}}$  near unity). Interestingly, the Base Case exhibits some small areas near the channel network where saturation-excess runoff is dominant ( $Q_{\text{inf}}/Q_{\text{tot}} < 0.5$ ), whereas the rest of the watershed is characterized by runoff generated exclusively when rainfall events exceed the infiltration capacity of the hillslope soils. As  $K_{\text{hill}}$  is increased (e.g., eolian sand deposition), the portion of the watershed producing saturation-excess runoff ( $Q_{\text{inf}}/Q_{\text{tot}} < 0.5$ ) expands into small tributaries and hillslope surfaces, in particular, for areas with higher rainfall amounts (see effects of Thiessen polygons shown in Figure 4c) and shrub cover due to higher hydraulic conductivities. This suggests that soils with a high  $K_{\text{hill}}$  and a limited depth of  $Z_r = 50$  cm receive sufficient rainfall during the summer season to generate saturation-excess runoff. In addition, the higher saturated hydraulic conductivities in hillslope soils bounded by an impermeable bottom allow for lateral subsurface flows that help to saturate the channel network, in effect creating a variable source area in the arid piedmont watershed. Note that the differences between the  $5K_{\text{hill}}$  and  $10K_{\text{hill}}$  cases are small and consistent with the low sensitivity of  $P/R$  over this range, while simulations that test values between  $K_{\text{hill}}$  and  $5K_{\text{hill}}$  exhibit a gradual change in the spatial patterns in  $Q_{\text{inf}}/Q_{\text{tot}}$  (i.e.,  $1.2 K_{\text{hill}}$ ,  $1.5K_{\text{hill}}$ , and  $2K_{\text{hill}}$ , not shown). Whether runoff production is dominated by infiltration- or saturation-excess types, we find that the hillslope infiltration capacity controls the rainfall threshold required for percolation losses to occur in the channel network, which are thus susceptible to changes in hillslope conditions, for instance, with respect to the woody plant encroachment process (e.g., Bestelmeyer et al., 2011; Gibbens et al., 2005).

## 4. Discussion

### 4.1. Confronting Numerical Simulations With Field-Derived Conceptual Models

While process-based, distributed hydrologic models have evolved considerably (see Fatichi et al., 2016), there is an urgent need to confront model formulations with long-term field observations from which a conceptual



model of hydrologic behavior has been developed (Beven, 2012). Conventional model evaluations are often limited to short periods of time (e.g., single events and seasonal variations), reducing the opportunities to capture the conceptual behavior or reproduce the full range of spatiotemporal variations in watershed conditions. This is particularly problematic in seasonally wet systems where a disproportional focus is placed on periods when hydrologic dynamics are most active (e.g., Moreno et al., 2013; Mueller et al., 2007; Vivoni et al., 2010). As noted here, extending simulations to seasons with lower hydrologic activity and across years with highly variable precipitation can yield important insights on model limitations. For instance, we identified an interaction between hillslope infiltration into calcium carbonate layers (Duniway et al., 2010) and springtime transpiration of deep-rooted mesquite shrubs (Reynolds et al., 1999) that is difficult to represent under the current modeling assumptions. Similar improvements are required to allow seasonal vegetation parameters to vary from year to year in response to climate conditions and for shrub patches to extend their roots underneath bare intercanopy spaces and draw water during periods of dry shallow soils (Heitschmidt et al., 1988).

Perhaps more importantly, the long-term observations of the water balance components revealed the critical role played by channel transmission losses in the arid piedmont slope. Direct measurements of channel losses are notoriously difficult (Goodrich et al., 2004; Shanafield & Cook, 2014) and have been used infrequently to test the performance of hydrologic models (but see Costa et al., 2012). In small watersheds, there are additional limitations in using streamflow differencing techniques to determine percolation (Schreiner-McGraw & Vivoni, 2017). As such, multiple lines of field evidence are needed to modify long-standing conceptualizations of watershed behavior (Tromble, 1988; Turnbull et al., 2013) that can subsequently form the basis for numerical model developments. As shown here, accounting for a short transient period of high channel infiltration losses (Blasch et al., 2006) is essential for reproducing monthly water balance residuals and the streamflow response at the watershed outlet. Nevertheless, additional modeling efforts will likely be required to link channel losses to vadose zone storage, plant water uptake, or recharge once field observations have been used to further refine the conceptual model of watershed behavior, leading to an iterative process of observational-modeling studies.

#### 4.2. Hillslope-Channel Connectivity in Arid Piedmont Slopes

The linkages between hillslopes and channels in arid and semiarid regions are generally poorly constrained in part due to the overall dry conditions that reduce their connectivity (e.g., Gutiérrez-Jurado et al., 2013; Puigdefabregas et al., 1998). While infiltration-excess runoff is the dominant mechanism in drylands (Yair & Lavee, 1985), its occurrence is limited to sporadic periods when sufficient rainfall allows hillslope-channel pathways to exceed losses and connect. Nevertheless, model sensitivity analyses reveal that a transition toward saturation-excess runoff is possible if hillslopes have high infiltration and are bounded by a shallow impermeable layer. While this transition does not affect the relation between percolation and rainfall, changes in the water balance would impact the watershed sensitivity to soil, vegetation, and terrain properties. For instance, the spatial distribution of the depth to the impermeable layer becomes more critical when saturation-excess runoff is an important mechanism (e.g., Lanni et al., 2013; Shi et al., 2015). As a result, the spatial continuity of the calcium carbonate layer is important to ascertain. Furthermore, a switch from infiltration- to saturation-excess runoff limits the sensitivity to infiltration differences between plant patches and bare soil areas but augments the effects of the partitioning between soil evaporation and plant transpiration. Since arid and semiarid plants are well adapted to extract available water (e.g., Gee et al., 1994), such a transition would yield increases in ET that reduce hydrologic connectivity via subsurface pathways.

In the context of arid piedmont slopes, it is important to recognize the role of hillslope-channel connectivity on streamflow yield and groundwater recharge. Snyder et al. (2006) and Bestelmeyer et al. (2011) suggest that coarse soils on piedmont surfaces might have substantial subsurface losses that disconnect them from downstream regions such as playas. As shown here, channel losses are mediated by the infiltration properties of hillslope surfaces, including the composition of vegetation patches and bare soil, such that state transitions (i.e., grassland to shrubland conversions, Gibbens et al., 2005) should impact the rainfall thresholds required to induce groundwater recharge. In addition, a modification of the hydrologic connectivity on hillslope surfaces, for instance, through restoration measures (Okin et al., 2015), would affect channel percolation and streamflow production. For the current plant assemblage in the mixed shrubland (Templeton et al., 2014), a rainfall event of 12.5 mm or greater is sufficient to produce hillslope runoff that is absorbed in the channel network prior to generating outlet streamflow. This model-derived threshold can be compared to the work of

McKenna and Sala (2018) also at the JER who found that rainfall events of 20 mm resulted in runoff reaching playas that were downstream of watersheds of much larger size, ranging from 0.1 to 48.9 km<sup>2</sup>. As a result, we expect that additional channel transmission losses occur between small watersheds on the arid piedmont slope and the larger catchments draining to playas.

## 5. Concluding Remarks

This study explores the sensitivity of hillslope runoff and channel transmission losses in an arid piedmont slope watershed as simulated by a distributed hydrologic model. Modifications were required in the model to account for hydrologic processes identified through extensive field sampling and an environmental sensor network. The novel combination of the high-resolution distributed data sets and numerical model allowed for an in-depth examination of the hillslope and channel processes explaining the partitioning of the water balance components. Hillslope and channel infiltration properties have varying effects on subsurface losses in arid piedmont slopes, with plausible combinations leading to dramatically different internal processes but similar hydrologic outcomes. As a result, the agreement between the field-derived conceptual model and the numerical simulations provides confidence that the modeling framework can be used to explore the effects of alternative vegetation states, restoration actions, or climate change-induced variability in meteorological forcing. Furthermore, the general patterns of watershed behavior emerging from this work may help guide studies in other arid piedmont slopes.

## Acknowledgments

We thank Dawn Browning and Naomi Robin Luna for providing the phenological data and John Anderson and other staff members of the USDA-ARS and Jornada LTER for field and data support. Funding provided by the Jornada LTER (DEB-1235828), Army Research Office (56059-EV-PCS), and USDA NIFA Graduate Fellowship program to A. S.-M. is acknowledged. We are grateful to R. C. Templeton, C. A. Anderson, and E. R. Pérez-Ruiz for their field activities. Data sets for the site are available at the Jornada Data Catalog (<http://jornada.nmsu.edu/lter/data>). We would like to thank two anonymous reviewers for their insightful comments that helped improve an initial version of the manuscript.

## References

- Abdulrazzak, M. J. (1995). Losses of flood water from alluvial channels. *Arid Land Resources Management*, 9(1), 15–24.
- Abdulrazzak, M. J., & Morel-Seytoux, H. (1983). Recharge from an ephemeral stream following wetting front arrival to water table. *Water Resources Research*, 19(1), 194–200. <https://doi.org/10.1029/WR019i001p00194>
- Abrahams, A. D., Neave, M., Schlesinger, W. H., Wainwright, J., Howe, D. A., & Parsons, A. J. (2006). Biogeochemical fluxes across piedmont slopes of the Jornada Basin. In K. M. Havstad, L. F. Huenneke, & W. H. Schlesinger (Eds.), *Structure and function of a Chihuahuan Desert ecosystem* (pp. 150–175). New York, NY: Oxford University Press.
- Anderson, C. A., & Vivoni, E. R. (2016). Impacts of land surface states within the flux footprint on daytime land-atmosphere coupling in two semiarid ecosystems of the southwestern U.S. *Water Resources Research*, 52, 4785–4800. <https://doi.org/10.1002/2015WR018016>
- Bestelmeyer, B. T., Goolsby, D. P., & Archer, S. R. (2011). Spatial perspectives in state-and-transition models: A missing link to land management? *Journal of Applied Ecology*, 48(3), 746–757. <https://doi.org/10.1111/j.1365-2664.2011.01982.x>
- Beven, K. J. (2012). *Rainfall-runoff modeling: The primer* (2nd ed., p. 488). West Sussex, UK: Wiley-Blackwell. <https://doi.org/10.1002/9781119951001>
- Blasch, K. W., Ferré, T. P. A., Hoffmann, J. P., & Fleming, J. B. (2006). Relative contributions of transient and steady state infiltration during ephemeral streamflow. *Water Resources Research*, 42, W08405. <https://doi.org/10.1029/2005WR004049>
- Coes, A. L., & Pool, D. R. (2005). Ephemeral-stream channel and basin-floor infiltration and recharge in the Sierra Vista subwatershed of the Upper San Pedro Basin, southeastern Arizona. U.S. Geological Survey Open-File Report 2005-1023, 67 pp.
- Costa, A. C., Bronstert, A., & de Araújo, J. C. (2012). A channel transmission losses model for different dryland rivers. *Hydrology and Earth System Sciences*, 16(4), 1111–1135. <https://doi.org/10.5194/hess-16-1111-2012>
- Dugas, W. A., Hicks, R. A., & Gibbens, R. P. (1996). Structure and function of C3 and C4 Chihuahuan Desert plant communities. Energy balance components. *Journal of Arid Environments*, 34(1), 63–79. <https://doi.org/10.1006/jare.1996.0093>
- Duniway, M., Herrick, J., & Monger, H. (2010). Spatial and temporal variability of plant-available water in calcium carbonate-cemented soils and consequences for arid ecosystem resilience. *Oecologia*, 163(1), 215–226. <https://doi.org/10.1007/s00442-009-1530-7>
- Faticchi, S., Vivoni, E. R., Ogden, F. L., Ivanov, V. Y., Mirus, B., Gochis, D., et al. (2016). An overview of current applications, challenges and future trends of distributed process-based models in hydrology. *Journal of Hydrology*, 537, 45–60. <https://doi.org/10.1016/j.jhydrol.2016.03.026>
- Frisbee, M. D., Allan, C. J., Thomasson, M. J., & Mackereth, R. (2007). Hillslope hydrology and wetlands response of two small zero-order boreal catchments on the Precambrian shield. *Hydrological Processes*, 21(22), 2979–2997. <https://doi.org/10.1002/hyp.6521>
- Garrote, L., & Bras, R. L. (1995). A distributed model for real-time flood forecasting using digital elevation models. *Journal of Hydrology*, 167(1–4), 279–306. [https://doi.org/10.1016/0022-1694\(94\)02592-Y](https://doi.org/10.1016/0022-1694(94)02592-Y)
- Gee, G. W., Wierenga, P. J., Andraski, B. J., Young, M. H., Fayer, M. J., & Rockhold, M. L. (1994). Variations in water balance and recharge potential at three western desert sites. *Soil Science Society of America Journal*, 58(1), 63–72. <https://doi.org/10.2136/sssaj1994.03615995005800010009x>
- Gibbens, R. P., McNeely, R. P., Havstad, K. M., Beck, R. F., & Nolen, B. (2005). Vegetation changes in the Jornada Basin from 1858 to 1998. *Journal of Arid Environments*, 61(4), 651–668. <https://doi.org/10.1016/j.jaridenv.2004.10.001>
- Goodrich, D. C., Lane, L. J., Shillito, R. M., Miller, S. N., Syed, K. H., & Woolhiser, D. A. (1997). Linearity of basin response as a function of scale in a semiarid watershed. *Water Resources Research*, 33(12), 2951–2965. <https://doi.org/10.1029/97WR01422>
- Goodrich, D. C., Williams, D. G., Unkrich, C. L., Hogan, J. F., Scott, R. L., Hultine, K. R., et al. (2004). Comparison of methods to estimate ephemeral channel recharge, Walnut Gulch, San Pedro River Basin, Arizona. In J. F. Hogan, F. M. Phillips, & B. R. Scanlon (Eds.), *Groundwater recharge in a desert environment* (pp. 77–99). Washington, DC: American Geophysical Union.
- Gutiérrez-Jurado, H. A., Vivoni, E. R., Cikoski, C., Harrison, J. B. J., Bras, R. L., & Istanbuluoglu, E. (2013). On the observed ecohydrologic dynamics of a semiarid basin with aspect-delimited ecosystems. *Water Resources Research*, 49, 8263–8284. <https://doi.org/10.1002/2013WR014364>
- Gutiérrez-Jurado, H. A., Vivoni, E. R., Istanbuluoglu, E., & Bras, R. L. (2007). Ecohydrological response to a geomorphically significant flood event in a semiarid catchment with contrasting ecosystems. *Geophysical Research Letters*, 34, L24525. <https://doi.org/10.1029/2007GL030994>

- Harms, D. (2015). US Department of Agriculture Soil Climate Analysis Network (SCAN) site 2168 data, Jornada Experimental Range, New Mexico. Ag Data Commons. <https://data.nal.usda.gov/dataset/us-department-agriculture-soil-climate-analysis-network-scan-site-2168-data-jornada-1>.
- Havstad, K. M., Huenneke, L. F., & Schlesinger, W. H. (2006). *Structure and function of a Chihuahuan Desert ecosystem: The Jornada Basin long-term ecological research site* (p. 492). New York, NY: Oxford Univ. Press.
- Hawkins, G. A., Vivoni, E. R., Robles-Morua, A., Mascaró, G., Rivera, E., & Dominguez, F. (2015). A climate change projection for summer hydrologic conditions in a semiarid watershed of central Arizona. *Journal of Arid Environments*, 118, 9–20. <https://doi.org/10.1016/j.jaridenv.2015.02.022>
- Heitschmidt, R. K., Ansley, R. J., Dowhower, S. L., Jacoby, P. W., & Price, D. L. (1988). Some observations from the excavation of honey mesquite root systems. *Journal of Range Management*, 41(3), 227–231. <https://doi.org/10.2307/3899173>
- Howes, D. A. (1999). Modeling runoff in a desert shrubland ecosystem, Jornada Basin, New Mexico, (PhD dissertation). Buffalo, NY: State University of New York at Buffalo.
- Howes, D. A., & Abrahams, A. D. (2003). Modeling runoff and runoff in a desert shrubland ecosystem, Jornada Basin, New Mexico. *Geomorphology*, 53(1-2), 45–73. [https://doi.org/10.1016/S0169-555X\(02\)00347-1](https://doi.org/10.1016/S0169-555X(02)00347-1)
- Ivanov, V. Y. (2002). A continuous Real-time Interactive Basin Simulator (RIBS). MS Thesis. Massachusetts Institute of Technology, Cambridge, MA, USA, 172 pp.
- Ivanov, V. Y., Vivoni, E. R., Bras, R. L., & Entekhabi, D. (2004). Catchment hydrologic response with a fully-distributed triangulated irregular network model. *Water Resources Research*, 40, W11102. <https://doi.org/10.1029/2004WR003218>
- Jencso, K. G., McGlynn, B. L., Gooseff, M. N., Wondzell, S. M., Bencala, K. E., & Marshall, L. A. (2009). Hydrologic connectivity between landscapes and streams: Transferring reach- and plot-scale understanding to the catchment scale. *Water Resources Research*, 45, W04428. <https://doi.org/10.1029/2008WR007225>
- Keppel, R. V., & Renard, K. G. (1962). Transmission losses in ephemeral streambeds. *Journal of hydraulic division of the American society of Civil Engineering*, 88, 59–68.
- King, W. E., & Hawley, J. W. (1975). Geology and ground-water resources of the Las Cruces area, New Mexico. Pages 195–204 In W. R. Seager, R. E. Clemons, & J. F. Callender (Eds.), *New Mexico Geological Society 26th Annual Fall Field Conference Guidebook* (376 pp.).
- Kirkby, M., Bracken, L., & Reaney, S. (2002). The influence of land use, soils and topography on the delivery of hillslope runoff to channels in SE Spain. *Earth Surface Processes and Landforms*, 27(13), 1459–1473. <https://doi.org/10.1002/esp.441>
- Lane, L. J. (1982). Distributed model for small semiarid basins. *Journal of Hydraulic Division of the American Society of Civil Engineers*, 108, 1114–1131.
- Lanni, C., McDonnell, J., Hopp, L., & Rigon, R. (2013). Simulated effects of soil depth and bedrock topography on near-surface hydrologic response and slope stability. *Earth Surface Processes and Landforms*, 38(2), 146–159. <https://doi.org/10.1002/esp.3267>
- Lekach, J., Amit, R., Grodek, T., & Schick, A. P. (1998). Fluvio-pedogenic processes in an ephemeral stream channel, Nahal Yael, southern Negev, Israel. *Geomorphology*, 23(2-4), 353–369. [https://doi.org/10.1016/S0169-555X\(98\)00015-4](https://doi.org/10.1016/S0169-555X(98)00015-4)
- Lin, H. S., Kogelmann, W., Walker, C., & Burns, M. A. (2006). Soil moisture patterns in a forested catchment: A hydropedological perspective. *Geoderma*, 131(3-4), 345–368. <https://doi.org/10.1016/j.geoderma.2005.03.013>
- Luna, N. R. (2016). Spatiotemporal variability of plant phenology in drylands: A case study from the northern Chihuahuan Desert. MS Thesis, University of Texas, El Paso. 100 pp.
- Mahmood, T. H., & Vivoni, E. R. (2011). A climate-induced threshold in hydrologic response in a semiarid ponderosa pine hillslope. *Water Resources Research*, 47, W09529. <https://doi.org/10.1029/2011WR010384>
- Manning, A. H., & Solomon, D. K. (2003). Using noble gases to investigate mountain-front recharge. *Journal of Hydrology*, 275(3-4), 194–207. [https://doi.org/10.1016/S0022-1694\(03\)00043-X](https://doi.org/10.1016/S0022-1694(03)00043-X)
- McCallum, A. M., Andersen, M. S., Rau, G. C., Larsen, J. R., & Acworth, R. I. (2014). River-aquifer interactions in a semiarid environment investigated using point and reach measurements. *Water Resources Research*, 50, 2815–2829. <https://doi.org/10.1002/2012WR012922>
- McKenna, O. P., & Sala, O. E. (2018). Groundwater recharge in desert playas: Current rates and future effects of climate change. *Environmental Research Letters*, 13(1), 014025. <https://doi.org/10.1088/1748-9326/aa9eb6>
- Méndez-Barroso, L. A., Vivoni, E. R., & Mascaró, G. (2016). Impact of spatially-variable soil thickness and texture on simulated hydrologic conditions in a semiarid watershed in northwest Mexico. *Revista Mexicana de Ciencias Geológicas*, 33(3), 365–377.
- Méndez-Barroso, L. A., Vivoni, E. R., Robles-Morua, A., Mascaró, G., Yopez, E. A., Rodríguez, J. C., et al. (2014). A modeling approach reveals differences in evapotranspiration and its partitioning in two semiarid ecosystems in Northwest Mexico. *Water Resources Research*, 50, 3229–3252. <https://doi.org/10.1002/2013WR014838>
- Monger, H. C. (2006). Soil development in the Jornada basin. In K. M. Havstad, L. F. Huenneke, & W. H. Schlesinger (Eds.), *Structure and function of a Chihuahuan Desert ecosystem* (pp. 81–106). New York, NY: Oxford University Press.
- Monger, H. C., Mack, G. H., Nolen, B. A., & Gile, L. H. (2006). Regional setting of the Jornada basin. In K. M. Havstad, L. F. Huenneke, & W. H. Schlesinger (Eds.), *Structure and function of a Chihuahuan Desert ecosystem* (pp. 15–43). New York, NY: Oxford University Press.
- Moreno, H. A., Vivoni, E. R., & Gochis, D. J. (2013). Limits to flood forecasting in the Colorado Front Range for two summer convection periods using radar nowcasting and a distributed hydrologic model. *Journal of Hydrometeorology*, 14(4), 1075–1097. <https://doi.org/10.1175/JHM-D-12-0129.1>
- Mueller, E. N., Wainwright, J., & Parsons, A. J. (2007). Impact of connectivity on the modeling of overland flow within semiarid shrubland environments. *Water Resources Research*, 43, W09412. <https://doi.org/10.1029/2006WR005006>
- Mukhopadhyay, B., Cornelius, J., & Zehner, W. (2003). Application of kinematic wave theory for predicting flash flood hazards on coupled alluvial fan-piedmont plain landforms. *Hydrological Processes*, 17, 838–868.
- Niswonger, R. G., Prudic, D. E., Pohl, G., & Constantz, J. (2005). Incorporating seepage losses into the unsteady streamflow equations for simulating intermittent flow along mountain front streams. *Water Resources Research*, 41, W06006. <https://doi.org/10.1029/2004WR003677>
- Okin, G. S., Moreno-de las Heras, M., Saco, P. M., Throop, H. L., Vivoni, E. R., Parsons, A. J., et al. (2015). Connectivity in dryland landscapes: Shifting concepts of spatial interactions. *Frontiers in Ecology and the Environment*, 13(1), 20–27. <https://doi.org/10.1890/140163>
- Osborn, H. B., & Renard, K. G. (1970). Thunderstorm runoff on the Walnut Gulch experimental watershed, Arizona, USA. In *The results of research on representative and experimental basins* (pp. 455–464). Wellington, New Zealand: Proc. IAHS-UNESCO Symposium.
- Parsons, A. J., Wainwright, J., Schlesinger, W. H., & Abrahams, A. D. (2003). The role of overland flow in sediment and nitrogen budgets of mesquite dunefields, southern New Mexico. *Journal of Arid Environments*, 53(1), 61–71. <https://doi.org/10.1006/jare.2002.1021>
- Parsons, A. J., Wainwright, J., Stone, P. M., & Abrahams, A. D. (1999). Transmission losses in rills on dryland hillslopes. *Hydrological Processes*, 13(17), 2897–2905. [https://doi.org/10.1002/\(SICI\)1099-1085\(19991215\)13:17<2897::AID-HYP905>3.0.CO;2-B](https://doi.org/10.1002/(SICI)1099-1085(19991215)13:17<2897::AID-HYP905>3.0.CO;2-B)

- Pelletier, J. D., Mayer, L., Pearthree, P. A., House, P. K., Demsey, K. A., Klawon, J. E., & Vincent, K. R. (2005). An integrated approach to flood hazard assessment on alluvial fans using numerical modeling, field mapping and remote sensing. *GSA Bulletin*, *117*(9), 1167–1180. <https://doi.org/10.1130/B25544.1>
- Peterson, F.F. 1981. Landforms of the basin and range province defined for soil survey. Reno, NV: Nevada Agricultural Experiment Station Technical Bulletin No. 28.52 pp.
- Pierini, N. A., Vivoni, E. R., Robles-Morua, A., Scott, R. L., & Nearing, M. A. (2014). Using observations and a distributed hydrologic model to explore runoff threshold processes linked with mesquite encroachment in the Sonoran Desert. *Water Resources Research*, *50*, 8191–8215. <https://doi.org/10.1002/2014WR015781>
- Pool, D. R. (2005). Variations in climate and ephemeral channel recharge in southeastern Arizona, United States. *Water Resources Research*, *41*, W11403. <https://doi.org/10.1029/2004WR00325>
- Puigdefabregas, J., del Barrio, G., Boer, M. M., Gutierrez, L., & Sole, A. (1998). Differential responses of hillslope and channel elements to rainfall events in a semi-arid area. *Geomorphology*, *23*(2–4), 337–351. [https://doi.org/10.1016/S0169-555X\(98\)00014-2](https://doi.org/10.1016/S0169-555X(98)00014-2)
- Rachal, D. M., Monger, H. C., Okin, G. S., & Peters, D. C. (2012). Landform influences on the resistance of grasslands to shrub encroachment, Northern Chihuahuan Desert, USA. *Journal of Maps*, *8*(4), 507–513. <https://doi.org/10.1080/17445647.2012.727593>
- Rawls, W. J., Brakensiek, D. L., & Miller, N. (1983). Green-ampt infiltration parameters from soil data. *Journal of Hydraulic Engineering*, *109*(1), 62–70. [https://doi.org/10.1061/\(ASCE\)0733-9429\(1983\)109:1\(62\)](https://doi.org/10.1061/(ASCE)0733-9429(1983)109:1(62))
- Renard, K. G., Nichols, M. H., Woolhiser, D. A., & Osborn, H. B. (2008). A brief background on the U.S. Department of Agriculture Agricultural Research Service Walnut Gulch Experimental Watershed. *Water Resources Research*, *44*, W05502. <https://doi.org/10.1029/2006WR005691>
- Rew, S. N., & McCuen, R. H. (2010). Analysis and synthesis of transmission loss hydrographs. *Journal of Irrigation and Drainage Engineering*, *136*(9), 637–645. [https://doi.org/10.1061/\(ASCE\)IR.1943-4774.0000228](https://doi.org/10.1061/(ASCE)IR.1943-4774.0000228)
- Reynolds, J. F., Virginia, R. A., Kemp, P. R., de Souza, A. G., & Tremmel, D. C. (1999). Impact of drought on desert shrubs: Effects of seasonality and degree of resource island development. *Ecological Monographs*, *69*(1), 69–106. [https://doi.org/10.1890/0012-9615\(1999\)069\[0069:IODODS\]2.0.CO;2](https://doi.org/10.1890/0012-9615(1999)069[0069:IODODS]2.0.CO;2)
- Rinehart, A. J., Vivoni, E. R., & Brooks, P. D. (2008). Effects of vegetation, albedo and solar radiation sheltering on the distribution of snow in the Valles Caldera, New Mexico. *Ecohydrology*, *1*(3), 253–270. <https://doi.org/10.1002/eco.26>
- Robins, C. R., Buck, B. J., Williams, A. J., Morton, J. L., House, P. K., Howell, M. S., & Yonovitz, M. L. (2009). Comparison of flood hazard assessments in desert piedmonts and playas: A case study in Ivanpah Valley, Nevada. *Geomorphology*, *103*(4), 520–532. <https://doi.org/10.1016/j.geomorph.2008.07.020>
- Robles-Morua, A., Vivoni, E. R., & Mayer, A. S. (2012). Distributed hydrologic modeling in northwest Mexico reveals the links between runoff mechanisms and evapotranspiration. *Journal of Hydrometeorology*, *13*(3), 785–807. <https://doi.org/10.1175/JHM-D-11-0112.1>
- Scanlon, B. R., Langford, R. P., & Goldsmith, R. S. (1999). Relationship between geomorphic settings and unsaturated flow in an arid setting. *Water Resources Research*, *35*(4), 983–999. <https://doi.org/10.1029/98WR02769>
- Schoener, G. (2017). Quantifying transmission losses in a New Mexico ephemeral stream: A losing proposition. *Journal of Hydrologic Engineering*, *22*(3), 05016038. [https://doi.org/10.1061/\(ASCE\)HE.1943-5584.0001473](https://doi.org/10.1061/(ASCE)HE.1943-5584.0001473)
- Schreiner-McGraw, A. P. (2017). Deep percolation in arid piedmont watersheds and its sensitivity to ecosystem change. PhD in Geological Sciences, Arizona State University, Tempe, AZ, USA, 282 pp.
- Schreiner-McGraw, A. P., & Vivoni, E. R. (2017). Percolation observations in an arid piedmont watershed and linkages to historical conditions in the Chihuahuan Desert. *Ecosphere*, *8*(11), e02000. <https://doi.org/10.1002/ecs2.2000>
- Schreiner-McGraw, A. P., Vivoni, E. R., Mascaró, G., & Franz, T. E. (2016). Closing the water balance with cosmic-ray soil moisture measurements and assessing their relation to evapotranspiration in two semiarid watersheds. *Hydrology and Earth System Sciences*, *20*(1), 329–345. <https://doi.org/10.5194/hess-20-329-2016>
- Scott, R. L. (2010). Using watershed water balance to evaluate the accuracy of eddy covariance evaporation measurements for three semiarid ecosystems. *Agricultural and Forest Meteorology*, *150*(2), 219–225. <https://doi.org/10.1016/j.agrformet.2009.11.002>
- Scott, R. L., Shuttleworth, W. J., Keefer, T. O., & Warrick, A. W. (2000). Modeling multiyear observations of soil moisture recharge in the semiarid American Southwest. *Water Resources Research*, *36*(8), 2233–2247. <https://doi.org/10.1029/2000WR900116>
- Seyfried, M. S., Schwinning, S., Walvoord, M. A., Pockman, W. T., Newman, B. D., Jackson, R. B., & Phillips, F. M. (2005). Ecohydrological controls of deep drainage in arid and semiarid regions. *Ecology*, *86*(2), 277–287. <https://doi.org/10.1890/03-0568>
- Shanfield, M., & Cook, P. G. (2014). Transmission losses, infiltration and groundwater recharge through ephemeral and intermittent streambeds: A review of applied methods. *Journal of Hydrology*, *511*, 518–529. <https://doi.org/10.1016/j.jhydrol.2014.01.068>
- Shentsis, I., & Rosenthal, E. (2003). Recharge of aquifers by flood events in an arid region. *Hydrological Processes*, *17*(4), 695–712. <https://doi.org/10.1002/hyp.1160>
- Shi, Y. N., Baldwin, D. C., Davis, K. J., Yu, X., Duffy, C. J., & Lin, H. (2015). Simulating high-resolution soil moisture patterns in the Shale Hill watershed using a land surface hydrologic model. *Hydrological Processes*, *29*(21), 4624–4637. <https://doi.org/10.1002/hyp.10593>
- Sidle, R. C., Tsuboyama, Y., Noguchi, S., Hosoda, I., Fujieda, M., & Shimizu, T. (2000). Stormflow generation in steep forested headwaters: A linked hydrogeomorphic paradigm. *Hydrological Processes*, *14*(3), 369–385. [https://doi.org/10.1002/\(SICI\)1099-1085\(20000228\)14:3<369::AID-HYP943>3.0.CO;2-P](https://doi.org/10.1002/(SICI)1099-1085(20000228)14:3<369::AID-HYP943>3.0.CO;2-P)
- Smith, R. E., Goodrich, D. C., Woolhiser, D. A., & Unkrich, C. L. (1995). KINEROS—A kinematic runoff and erosion model. In V. J. Singh (Ed.), *Computer models of watershed hydrology* (pp. 697–732). Highlands Ranch, Colorado: Water Resources Publications.
- Smith, R. W., Chery, D. L., Renard, K. G., & Gwinn, W. R. (1981). *Supercritical flow flumes for measuring sediment-laden flow*, Technical Bulletin 1655 (p. 70). Washington, DC: US Government Printing Office.
- Smith, S. D., Herr, C. A., Leary, K. L., & Piorkowski, J. M. (1995). Soil-plant water relations in a Mojave Desert mixed shrub community: A comparison of three geomorphic surfaces. *Journal of Arid Environments*, *29*(3), 339–351. [https://doi.org/10.1016/S0140-1963\(05\)80113-2](https://doi.org/10.1016/S0140-1963(05)80113-2)
- Snyder, K. A., Mitchell, K. A., & Herrick, J. E. (2006). Patterns and controls of soil water in the Jornada Basin. In K. M. Havstad, L. F. Hueneke, & W. H. Schlesinger (Eds.), *Structure and function of a Chihuahuan Desert ecosystem* (pp. 107–132). New York, NY: Oxford University Press.
- Sonnentag, O., Hufkens, K., Teshera-Sterne, C., Young, A. M., Friedl, M., Braswell, B. H., et al. (2012). Digital repeat photography for phenological research in forest ecosystems. *Agricultural and Forest Meteorology*, *152*, 159–177. <https://doi.org/10.1016/j.agrformet.2011.09.009>
- Sorman, A. U., & Abdulrazzak, M. J. (1993). Infiltration-recharge through wadi beds in arid regions. *Hydrological Sciences Journal*, *38*(3), 173–186. <https://doi.org/10.1080/02626669309492661>
- Templeton, R. C., Vivoni, E. R., Méndez-Barroso, L. A., Pierini, N. A., Anderson, C. A., Rango, A., et al. (2014). High-resolution characterization of a semiarid watershed: Implications on evapotranspiration estimates. *Journal of Hydrology*, *509*, 306–319. <https://doi.org/10.1016/j.jhydrol.2013.11.047>



- Tooth, S. (2000). Process, form and change in dryland rivers: A review of recent research. *Earth-Science Reviews*, 51(1-4), 67–107. [https://doi.org/10.1016/S0012-8252\(00\)00014-3](https://doi.org/10.1016/S0012-8252(00)00014-3)
- Tromble, J. M. (1988). Water budget for creosotebush-infested rangeland. *Journal of Arid Environments*, 15, 71–74.
- Tromble, J. M., Renard, K. G., & Thatcher, A. P. (1974). Infiltration for three rangelands oil-vegetation complexes. *Journal of Range Management*, 27(4), 318–321. <https://doi.org/10.2307/3896834>
- Turnbull, L., Parsons, A. J., & Wainwright, J. (2013). Runoff responses to long-term rainfall variability in creosotebush-dominated shrubland. *Journal of Arid Environments*, 91, 88–94. <https://doi.org/10.1016/j.jaridenv.2012.12.002>
- Twine, T. E., Kustas, W. P., Norman, J. M., Cook, D. R., Houser, P. R., Meyers, T. P., et al. (2000). Correcting eddy-covariance flux underestimates over a grassland. *Agricultural and Forest Meteorology*, 103(3), 279–300. [https://doi.org/10.1016/S0168-1923\(00\)00123-4](https://doi.org/10.1016/S0168-1923(00)00123-4)
- Villeneuve, S., Cook, P. G., Shanfield, M., Wood, C., & White, N. (2015). Groundwater recharge via infiltration through an ephemeral riverbed, central Australia. *Journal of Arid Environments*, 117, 47–58. <https://doi.org/10.1016/j.jaridenv.2015.02.009>
- Vivoni, E. R. (2012). Spatial patterns, processes and predictions in ecohydrology: Integrating technologies to meet the challenge. *Ecohydrology*, 5(3), 235–241. <https://doi.org/10.1002/eco.1248>
- Vivoni, E. R., Entekhabi, D., Bras, R. L., & Ivanov, V. Y. (2007). Controls on runoff generation and scale-dependence in a distributed hydrologic model. *Hydrology and Earth System Sciences*, 11(5), 1683–1701. <https://doi.org/10.5194/hess-11-1683-2007>
- Vivoni, E. R., Ivanov, V. Y., Bras, R. L., & Entekhabi, D. (2004). Generation of triangulated irregular networks based on hydrological similarity. *Journal of Hydrologic Engineering*, 9(4), 288–302. [https://doi.org/10.1061/\(ASCE\)1084-0699\(2004\)9:4\(288\)](https://doi.org/10.1061/(ASCE)1084-0699(2004)9:4(288))
- Vivoni, E. R., Mascaró, G., Mniszewski, S., Fasel, P., Springer, E. P., Ivanov, V. Y., & Bras, R. L. (2011). Real-world hydrologic assessment of a fully-distributed hydrological model in a parallel computing environment. *Journal of Hydrology*, 409(1-2), 483–496. <https://doi.org/10.1016/j.jhydrol.2011.08.053>
- Vivoni, E. R., Moreno, H. A., Mascaró, G., Rodríguez, J. C., Watts, C. J., Garatuza-Payán, J., & Scott, R. L. (2008). Observed relation between evapotranspiration and soil moisture in the North American monsoon region. *Geophysical Research Letters*, 35, L22403. <https://doi.org/10.1029/2008GL036001>
- Vivoni, E. R., Rango, A., Anderson, C. A., Pierini, N. A., Schreiner-McGraw, A., Saripalli, S., & Laliberte, A. S. (2014). Ecohydrology with unmanned aerial vehicles. *Ecosphere*, 5(10), art130. <https://doi.org/10.1890/ES14-00217.1>
- Vivoni, E. R., Rodríguez, J. C., & Watts, C. J. (2010). On the Spatiotemporal Variability of Soil Moisture and Evapotranspiration in a Mountainous Basin within the North American Monsoon Region. *Water Resources Research*, 46, W02509. <https://doi.org/10.1029/2009WR008240>
- Wainwright, J. (2006). Climate and climatological variations in the Jornada Basin. In K. M. Havstad, L. F. Huenneke, & W. H. Schlesinger (Eds.), *Structure and function of a Chihuahuan Desert ecosystem* (pp. 44–80). New York, NY: Oxford University Press.
- Wainwright, J., Parsons, A. J., & Abrahams, A. D. (2000). Plot-scale studies of vegetation, overland flow and erosion interactions: Case studies from Arizona and New Mexico. *Hydrological Processes*, 14(16-17), 2921–2943. [https://doi.org/10.1002/1099-1085\(200011/12\)14:16/17<2921::AID-HYP127>3.0.CO;2-7](https://doi.org/10.1002/1099-1085(200011/12)14:16/17<2921::AID-HYP127>3.0.CO;2-7)
- Wainwright, J., Parsons, A. J., Schlesinger, W. H., & Abrahams, A. D. (2002). Hydrology-vegetation interactions in areas of discontinuous flow on a semi-arid bajada, southern New Mexico. *Journal of Arid Environments*, 51(3), 319–338. <https://doi.org/10.1006/jare.2002.0970>
- Walters, M. O. (1990). Transmission losses in arid region. *Journal of Hydraulic Engineering*, 116(1), 129–138.
- Wilson, J. L., & Guan, H. (2004). Mountain-block hydrology and mountain-front recharge. In J. F. Hogan, F. M. Phillips, & B. R. Scanlon (Eds.), *Groundwater recharge in a desert environment* (pp. 113–135). Washington, DC: American Geophysical Union.
- Wondzell, S. M., Cunningham, G. L., & Bachelet, D. (1996). Relationships between landforms, geomorphic processes, and plant communities on a watershed in the northern Chihuahuan Desert. *Landscape Ecology*, 11(6), 351–362. <https://doi.org/10.1007/BF02447522>
- Xiang, T. T., Vivoni, E. R., & Gochis, D. J. (2014). Seasonal evolution of ecohydrological controls on land surface temperature over complex terrain. *Water Resources Research*, 50(5), 3852–3874.
- Yair, A., & Lavee, H. (1985). Runoff generation in arid and semi-arid zones. In M. G. Anderson & T. P. Burt (Eds.), *Hydrological forecasting* (pp. 183–220). Chichester, UK: John Wiley.
- Young, M. H., McDonald, V., Caldwell, T. G., Benner, S. G., & Meadows, D. G. (2004). Hydraulic properties of a desert soil chronosequence in the Mojave Desert, USA. *Vadose Zone Journal*, 3(3), 956–963. <https://doi.org/10.2136/vzj2004.0956>